

The physical mechanisms of induced earthquakes

Mohammad J. A. Moein¹✉, Cornelius Langenbruch¹, Ryan Schultz^{2,3}, Francesco Grigoli⁴, William L. Ellsworth², Ruijia Wang⁵, Antonio Pio Rinaldi³ & Serge Shapiro¹

Abstract

Anthropogenic operations involving underground fluid extraction or injection can cause unexpectedly large and even damaging earthquakes, despite operational and regulatory efforts. In this Review, we explore the physical mechanisms of induced seismicity and their fundamental applications to modelling, forecasting, monitoring and mitigating induced earthquakes. The primary mechanisms of injection-induced earthquakes considered important for creating stress perturbations include pore-pressure diffusion, poroelastic coupling, thermoelastic stresses, earthquake interactions and aseismic slip. Extraction-induced earthquakes are triggered by differential compaction linked with poroelastic effects and reservoir creep. Secondary mechanisms include reducing the rock mass strength subject to stress corrosion, dynamic weakening and cohesion loss. However, constraining the maximum magnitude, M_{\max} , of a potential earthquake on the basis of physical process understanding is still challenging. Common M_{\max} theories are based on injection volume as the single source of strain, which might not be efficient in seismically active regions. Alternative time-based M_{\max} models have the potential to explain why some induced earthquake events tap into tectonic strain and lead to runaway ruptures (in which the rupture front extends beyond the perturbed rock volume). Developments in physics-based forecasting and potential future success in mitigation of induced-seismic risk could help increase the acceptance of emerging energy technologies such as enhanced geothermal systems and underground gas storage during the sustainable transition.

Sections

Introduction

Activities associated with induced earthquakes

Earthquake triggering mechanisms

Maximum induced earthquake magnitude

Monitoring, discrimination, risk, hazard and mitigation

Summary and future directions

¹Department of Earth Sciences, Free University of Berlin, Berlin, Germany. ²Department of Geophysics, Stanford University, Stanford, CA, USA. ³Department of Earth Sciences, ETH Zurich, Zurich, Switzerland.

⁴Department of Earth Sciences, University of Pisa, Pisa, Italy. ⁵Department of Earth and Space Sciences, Southern University of Science and Technology, Shenzhen, China. ✉e-mail: mohammad.moein@geophysik.fu-berlin.de

Key points

- Induced earthquakes are primarily triggered by stress perturbations that destabilize pre-existing critically stressed faults. However, industrial operations can also reactivate faults that were not initially critically stressed.
- The major triggering mechanism of injection-induced seismicity is pore-pressure diffusion, which reduces the normal stress acting on fractures and fault planes. The main mechanism of extraction-induced seismicity is poroelasticity, which affects the stress field in the surrounding rock formations and can trigger earthquakes.
- The occurrence of large-magnitude-induced earthquake events supports the hypothesis that the maximum earthquake magnitude is likely controlled by regional tectonics. Particularly, in seismically active regions, the tectonic source of strain often controls the extent of rupture on critically stressed faults.
- Fluid injection volume is not the only controlling parameter of maximum earthquake magnitude, and other factors such as the time elapsed from beginning of fluid extraction or injection (the triggering time) might have a substantial role. Triggering time is likely related to the time required to perturb the stress or strength of pre-existing faults.
- Accurate estimates of maximum magnitude can be aided when an inventory of pre-existing critically stressed faults, detailed in situ stress information and a physical understanding of the processes that control the rupture dynamics are available.
- Experiments in in situ underground laboratories with extensive monitoring systems and well-characterized rock mass provide a unique opportunity to test the methodological advances in managing seismicity and the effectiveness of numerical models at resolving coupled processes.

Introduction

The occurrence of moderate-to-large-magnitude-induced earthquakes (magnitudes above 4) has created negative social, environmental and economic consequences. Such earthquakes can be felt by the public, damage surface infrastructures, cause casualties and lead to the suspension of the industrial projects^{1–3}. Potential causes include anthropogenic activities such as water impoundment behind dams, geothermal developments, hydraulic fracturing of unconventional hydrocarbon reservoirs, conventional hydrocarbon recovery, wastewater disposal (WWD), underground gas or CO₂ storage (UGS) and mining operations⁴ (Fig. 1).

Many documented induced earthquakes were explained by the seismogenic response of subsurface reservoirs to injection or extraction^{5,6} and the maximum magnitudes M_{\max} were comparable to that of natural ones (namely, magnitudes above 4). Hence, it is relevant to understand the physical processes governing these earthquakes and develop strategies that forecast, control and mitigate the seismic risk. Since 2015, some notable advances have improved the current understanding of induced seismicity. In situ experiments with extensive monitoring systems and well-characterized rock mass were performed

in underground laboratories to bridge the gap between the small-scale laboratory and field-scale experiments^{7–9}. Methodological progress in small-scale experiments (both in laboratory and underground in situ experiments)¹⁰, large-scale operations¹¹ and risk-informed traffic light protocols (TLPs)¹² were achieved to reduce the seismicity and to enhance the current risk management capabilities. Also, theoretical developments in physical understanding of M_{\max} have explained the occurrence of large magnitude induced event such as in Pohang, South Korea 2017^{13,14}. Despite these advances, the occurrence of unexpectedly large (such as $M \geq 4$) induced events cannot be excluded.

Previous reviews have covered topics such as monitoring^{15,16}, modelling¹⁷ and controlling¹⁰ induced seismicity. Other reviews cover the seismological or geological aspects with a particular focus on a single application such as hydraulic fracturing^{18,19}, hydrocarbon recovery²⁰, WWD^{21,22}, enhanced geothermal systems (EGS)^{23,24}, mining²⁵ and UGS^{26,27}. However, there is a need for a process-based and mechanistic review of induced earthquakes more generally, with a particular focus on available M_{\max} theories and the broad implications for monitoring, discrimination between natural and induced earthquakes, hazard and risk assessments and mitigation strategies.

In this Review, we provide a brief and comprehensive overview of the physical processes governing fluid-induced (by injection or extraction) earthquakes. We place a specific focus on the triggering mechanisms and discuss the M_{\max} models in relation to physical processes. Then, we outline the implications of physics-based approaches for monitoring, discrimination, seismic risk and hazard assessment and mitigation strategies. Finally, we highlight emerging research directions to shape future developments to improve the current understanding of induced earthquakes, minimize their negative consequences and increase the acceptance of innovative energy technologies.

Activities associated with induced earthquakes

Globally, more than 50% of the industrial projects that were associated with anthropogenic earthquakes were directly linked to underground fluid injection or extraction. Among them, a notable number of cases have induced earthquakes exceeding M3 (Fig. 2). Here, we briefly discuss these activities and point out some of the largest events that occurred since 2010 (Table 1).

Enhanced geothermal systems

Geothermal energy aims to exploit the vast unexploited amount of heat stored in the crust that could be extracted by circulating fluids (such as water) between injection and extraction wells. Despite hydrothermal-type geothermal reservoirs, EGS technology aims to exploit the heat stored in high temperature formations with insufficient permeabilities. Such condition is typically met at the depths of 3–5 km, where the host formation is composed of low-permeability crystalline basement rocks. High-pressure fluid injection, known as hydraulic stimulation, is often carried out to create a subsurface heat exchanger. Hydraulic stimulation activates multiple physical processes²³ that create a high-permeability connection between the input and output wells. However, hydraulic stimulation is often associated with induced seismicity. The M_w 5.4 Pohang 2017, South Korea, was triggered by hydraulic stimulation of the close-by EGS project²⁸. Moreover, numerous small-to-moderate events (that is, $M > 3$) have been felt by public (Fig. 2), raising concern and threatening the social license to operate^{29,30}.

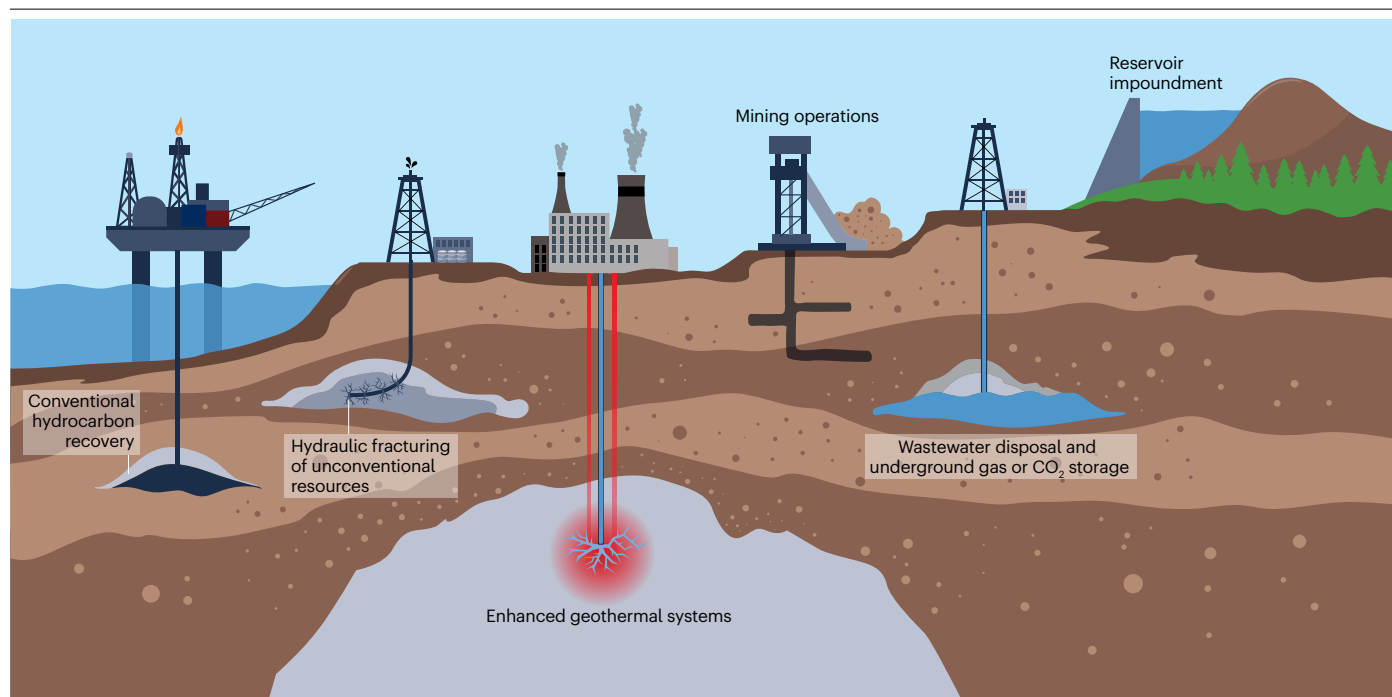


Fig. 1 | Industrial activities that can cause induced seismicity. Induced earthquakes can occur during conventional hydrocarbon recovery, hydraulic fracturing of unconventional resources, enhanced geothermal systems, mining

operations, wastewater disposal, underground gas or CO₂ storage operations and reservoir impoundment. Figure adapted with permission from ref. 16, Wiley.

The physical processes in EGS reservoirs are rather complex. If the temperature of the injected fluid and that of the reservoir are close (such as underground laboratories), one could anticipate that the dominant hydromechanical processes are not substantially influenced by the thermal component. The high temperature in such systems can exert over-closure of fractures and faults (namely, a better fit of the opposing walls causing an increase of frictional strength), which can be released by cooling, causing contraction effects³¹. Fluid injection or circulation can also disturb the geochemical equilibrium, with fluid–rock interactions potentially playing an important role in long-term operations. However, such rock–fluid interactions might be negligible over short-term injection operations¹⁷.

Hydraulic fracturing

Unconventional oil and gas reservoirs are often located in low-permeability formations such as shale. Extended reach horizontal wells, up to several kilometres in length, are hydraulically fractured at multiple intervals to create flow paths for oil and gas when the well is under production (namely, ‘flow-back’). Here, the objective is to generate a connected fracture network that facilitates hydrocarbon withdrawal. In such environments, hydromechanical processes influence both hydraulic fracture propagation and damage evolution, which controls the dimensions of hydraulic fracture and attendant seismicity³². Although it is widely observed that the generation of new fractures do not produce noticeable seismic magnitudes³³, pre-existing fractures and faults can be reactivated^{19,34} and cause felt events, even at relatively large distances³⁵. It is important to note that many shale plays did not encounter any M3+ events at all. At the basin scale in seismogenic shale plays, approximately 0.1–1% of the hydraulic fracturing wells were

associated with substantial induced earthquakes (namely, $M > 3$)³⁶. In Eastern Ohio USA, this percentage is approximately 10–33% (ref. 37). Yet, these percentages can vary substantially by location within the shale play. For example, the Duvernay play in Canada had percentages up to 10% in the most seismically active areas³⁸. However, the susceptibility of a location to encounter induced seismicity depends on many factors, including the geological conditions and the proximity to seismogenic and hydraulically active faults^{39,40}. Two notable M_s 6 and M_w 5.7 earthquakes in Luxian 2021 and Sichuan Basin 2019, both in China, were speculated to be linked with hydraulic fracturing of unconventional resources^{41,42}. Also, the M_w 4.6 earthquake in northwest of Fort St John, British Columbia 2015 was the largest induced event caused by hydraulic fracturing in Canada⁴³.

Wastewater disposal

The exploitation of petroleum resources produces large volumes of wastewater, which are typically disposed of via subsurface injection. WWD usually targets porous rocks in sedimentary layers, to store large volumes that can exceed 10^6 m³. In the corresponding formations, temperature and composition of injected fluid could be variable and require considering coupled processes⁴⁴. Some large magnitude ($M \geq 5$) earthquakes were likely related to WWD injections. An M_w 5.1 in Peace River, Alberta, Canada 2022 was likely related to the WWD of in situ bitumen recovery⁴⁵. The M_w 5 earthquakes in the Permian Basin of West Texas 2020, USA were potentially induced by nearby WWD operations⁴⁶. Also, three earthquakes of M_w 5.8, 5.1 and 5.7 occurred in Pawnee (2016), Fairview (2016) and Prague (2011) OK USA, respectively, were also caused by WWD associated with unconventional hydrocarbon production^{47,48}.

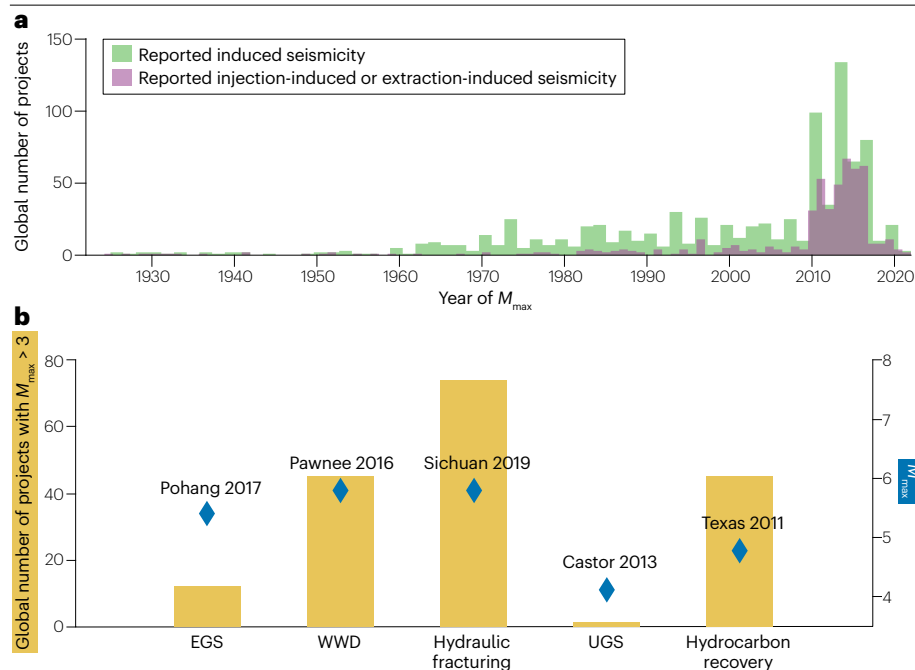


Fig. 2 | Increase in induced seismicity related to industrial operations. **a**, Global number of documented industrial projects associated with anthropogenic earthquakes compared with the number of fluid injection-induced or extraction-induced earthquakes. **b**, The number of reported induced earthquake events with $M_{\max} \geq 3$ in industrial operations dealing with fluid injection or extraction (yellow bars, left axis). The largest reported M_{\max} for each of the corresponding industrial operations since 2010 (blue diamonds, right axis). EGS, enhanced geothermal systems; UGS, underground gas or CO₂ storage; WWD, wastewater disposal. Data are from the Human-Induced Earthquake Database (HiQuake)²¹⁶.

Underground gas storage

Similar to WWD operations, UGS targets high-permeability porous rocks. High-permeability formations are typically selected to store large volumes (million tons) of gas or CO₂ in the subsurface. In such systems, the hydraulic processes are controlled by the multiphase mixture of the fluid, where the overpressure dissipates by pressure gradients and buoyancy forces. In the case of CO₂ storage, the fluid is typically injected in supercritical conditions and the transport occurs in a multiphase mixture. As CO₂ can disturb the geochemical equilibrium, the fluid–rock interactions can restructure the pore space by mineral dissolution and precipitation. These interactions change the permeability, porosity and poroelastic properties of the host formation. The most remarkable case history is the Castor project in offshore Spain, which triggered three M4.1 earthquakes in 2013^{49,50}. However, very few UGS projects reported induced seismicity.

Hydrocarbon recovery

Conventional hydrocarbon recovery from sedimentary rocks depressurizes the underground reservoirs. During the fluid extraction, the reservoir pressure drops and the elastic stresses become activated. One major challenge arises from the multiphase nature of fluids in geological systems (including oil, gas and water) and the chemical interactions among different phases⁵¹. During fluid extraction, the temperature of the reservoir system is not disturbed by external sources, the thermal interaction between the rock and fluid might not be substantial. The M_w 4.8 earthquake in the Eagle Ford Shale, TX, USA (2011) is one example of seismicity that was exclusively caused by hydrocarbon recovery⁵². Also, prominent case histories of Groningen gas field, The Netherlands^{53–57} and Lacq gas field, France^{58,59} are examples of extraction-induced seismicity in seismically quiet regions.

The maximum observed magnitude of induced earthquakes during underground fluid injection and extraction experiments varied between 4 and 6. Various operations target different geological

formations and operational variants that control the magnitude of induced earthquakes.

Earthquake triggering mechanisms

The primary triggering mechanisms of induced earthquakes (Box 1) considered important for creating stress perturbations include pore-pressure diffusion, poroelastic coupling, thermoelastic stresses, earthquake interactions and aseismic slip. Fault-weakening processes via chemical and physical processes can also expedite fluid–rock interactions and/or promote further instabilities. However, unravelling the influence of a single mechanism is challenging, as multiple mechanisms likely contribute to a single seismic event.

Stress perturbation

Pore-pressure changes. Pore-pressure changes and propagation are the primary mechanisms for inducing earthquakes⁶⁰. Often, the process of pore-pressure propagation is referred to as pressure diffusion as the equation governing such propagation can be approximated with a diffusion equation, assuming constant fluid density. When the fluid enters pre-existing fractures and faults, the rise in pore pressure supports a fraction of the normal stress and the effective normal stress is reduced – bringing the fault closer to the failure. Pressure changes can be transmitted far beyond the injection zone, up to tens of kilometres in highly permeable formations^{61–64}.

Pore-pressure diffusion has been identified as the primary mechanism for earthquakes induced by WWD, often many kilometres from the injection point, for which substantial seismicity can be delayed by months or longer^{62,65}. Earthquakes induced during EGS stimulations also primarily initiate in response to pore-pressure diffusion⁶⁶. During hydraulic fracturing, the pressure front outside the fractures is inhibited by the low permeability of the reservoir. Therefore, a hydrologic connection is required to transfer the pressure diffusion to critically stressed faults, on which dynamic rupture occurs.

This connection is likely provided by pre-existing fracture corridors that allowed communication of fluid-pressure perturbations to larger faults, even in distances more than 1 km (ref. 67). Most case histories of hydraulic fracturing are ascribed by the pore-pressure diffusion and hydraulic connection to the nearby faults^{36,68,69}. Hence, the proximity to the deep basement is a substantial geological factor when faults in crystalline basement become involved. The hydraulic connection and pressure migration to deeper formations have also been observed in the cases of WWD and UGS^{49,70,71}. However, pressure diffusion can also reactivate the faults in shallower depths of the injection point⁷².

Poroelastic coupling. Poroelastic stresses created by injection are also a triggering mechanism for either injection-induced or extraction-induced seismicity. During injection, seismicity is sometimes observed to outpace the pore-pressure front. Pressure diffusion cannot explain such seismicity unless high permeability fractures are present. Poroelastic stress transfer occurs at the speed of seismic waves and perturbs the strength balance on distant fractures and faults without any hydraulic communication⁷³. Poroelastic stress transfer results from overburden changes and pressurized expansion of the rock volume, which further trigger distant stress-induced pore-pressure changes. Although the stress perturbation owing to poroelastic effects is relatively small and diminishes with distance⁷⁴, it can be sufficient to awaken critically stressed fractures and faults in offset locations. Investigations have revealed that shear stress changes as small as 0.01–0.1 MPa can trigger seismic events⁷⁵. However, some authors reported perturbations as small as a few kilopascals⁷⁶. This threshold of stress perturbation is likely bounded by the Earth tidal stresses that rarely induce natural earthquakes⁷⁷. The role of poroelastic stress transfer has been discussed during geothermal developments^{78,79}, hydraulic fracturing operations^{34,72}, WWD^{80,81} and UGS⁸².

Fluid extraction reduces the pore pressure, which causes reservoir depletion and/or compaction. In comparison to fluid injection, extraction-induced seismicity can seem counterintuitive as fluid extraction generates negative pressure change (and thus increases fault stability). However, this argument is incomplete. Reservoir depletion and/or compaction also create high-stress regions surrounding the extraction volume that might eventually fail and trigger earthquakes⁸³. As the reservoir formation cannot contract freely in response to the fluid extraction, horizontal contraction within the reservoir generates differential stresses⁸⁴. The onset of compaction-induced seismicity in some cases can require a considerable pore-pressure drop of -10 MPa (refs. 51,85). Higher thresholds of stress perturbations support the viewpoint that the fluid production can reactivate faults that were not critically stressed before operation⁸⁶. Reservoir compaction also manifests itself as surface subsidence seen in deformation on the surface⁸⁷. Several prominent cases of extraction-induced seismicity were explained by the heterogeneously distributed strain^{56,58,88,89}.

Thermal stresses. When the temperature of injection fluid differs from the in situ temperature, thermal stresses can contribute to mechanical instability. Fluid injection into subsurface cools down the reservoir and generates contractional strain. The magnitude of thermal stress depends on the stiffness of the reservoir rock, becoming more important in stiffer formations⁹⁰. However, it is difficult to determine the contribution of thermal stresses during in situ injection experiments⁹¹. The thermal drawdown front is often slower than that of pore pressure⁹². Moreover, the thermal stresses can be transmitted

beyond the cooled region and destabilize faults in distant locations⁹³. Therefore, thermal effects are likely more important at later times than at the start of injection, but could have a critical role in the long run⁹⁴. The triggering of induced seismicity by thermal stresses was explored in several case histories during EGS stimulations^{95–97} and CO₂ storage⁹⁸.

Earthquake interactions. When an earthquake occurs, static stress along a fault changes near the rupture front⁹⁹, potentially advancing or retarding the generation of new earthquakes. This mechanism is known as earthquake interaction. Earthquakes also interact through the stress carried by the radiated waves, which are capable of triggering distant events – even in the stress shadow of the static field¹⁰⁰. Both static and dynamic mechanisms contribute to the occurrence of natural and induced earthquake sequences. According to rate-and-state theory¹⁰¹, the time it takes for the system to evolve to failure after perturbation depends nonlinearly on the initial state, size of the perturbation and stressing rate. Hence, failure can be nearly instantaneous or delayed by months or longer, giving rise to the spectrum of spatial and temporal clustering of seismicity seen in both natural and induced earthquakes¹⁰². Therefore, it can be difficult to assign causality between an industrial action and a specific earthquake when there are multiple sources of perturbations. In addition to the stress transfer of earlier earthquakes, the tensile opening of fractures generates an extrastatic stress that can generate a sequence of events that control the spatial distribution of seismic events, specifically during hydraulic fracturing

Table 1 | A selection of induced earthquakes caused by fluid injection and extraction

Induced earthquake event	Country	M_{\max}
Enhanced geothermal systems		
Pohang, 2017 ²⁸	South Korea	5.4
Strasbourg, 2020 ³⁰	France	3.9 (M_L)
Cooper Basin, 2012 ²¹³	Australia	3.7
Hydraulic fracturing		
Luxian, 2021 ⁴¹	China	6 (M_S)
Sichuan Basin, 2019 ²¹⁴	China	5.8
Fort St John, 2018 ²¹⁵	Canada	4.6
Wastewater disposal		
Pawnee, OK, 2016 ^{47,48}	USA	5.8
Peace River, 2022 ⁴⁵	Canada	5.1
Mentone, TX, 2020 ⁴⁶	USA	5
Hydrocarbon recovery		
Fashioning, TX, 2011 ⁵²	USA	4.8
Lacq, 2016 ⁵⁸	France	3.9
Groningen, 2012 ⁵⁵	The Netherlands	3.6 (M_L)
Underground gas storage		
Castor, 2013 ⁴⁹	Spain	4.1

The largest induced earthquake magnitudes documented for each type of industrial activity since 2010. For each activity, three examples are listed except underground gas storage, for which very few cases are reported. All of the reported M_{\max} values are moment magnitudes (M_w), unless otherwise stated. M_L is the local magnitude, M_{L_v} is the local magnitude measured on the vertical component and M_s is the surface wave magnitude.

Box 1

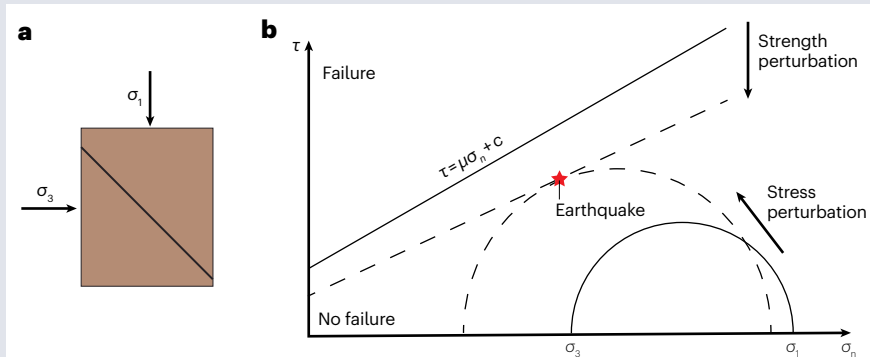
Earthquake nucleation and anthropogenic earthquakes

Earthquake nucleation

Earthquakes release strain energy by slip on pre-existing faults when the applied stresses exceed the frictional strength of the fault²¹⁷ (see the figure, right panel). The strain energy accumulates slowly, over decades to centuries on plate boundaries and over millennia in plate interiors. The nucleation zone for crustal earthquakes can be exceedingly small, with dimensions of less than a metre to a few tens of metres²¹⁸. Thus, perturbing only a very limited area on the fault can be sufficient to initiate an earthquake, for example, by raising the pore pressure and/or reducing the effective normal stress (see the figure). Once underway, the magnitude of the event is controlled by the prestress, geometry of the fault and size of the perturbation and has potential to rupture far beyond the nucleation zone^{142,150,219}.

Fundamentals of fault reactivation

The failure conditions of a fault are defined by the Mohr–Coulomb theory²²⁰ (see the figure, right panel), which are met when the shear stress acting on a fault plane exceeds the frictional strength of the fault, triggering an earthquake (red star). The in situ stresses acting on a fault plane include sigma 1, representing the principal or greatest compressive stress, and sigma 3, representing the least principal stress (see the figure, left panel). These minimum and maximum principal stress components can be plotted (solid semicircle) along with the Mohr–Coulomb criterion (solid line), which defines the failure conditions. If the shear stress, τ , acting on a fault plane exceeds the shear strength, which is a sum of frictional resistance $\mu\sigma_n$ and cohesion c , then failure occurs (the Mohr circle cuts the failure line, dashed semicircle and line). Any perturbations of in situ stress can change the radius and centre of the Mohr circle, moving it closer to the shear strength. In addition, a reduction of the friction coefficient μ and/or cohesion can reduce the strength of the fault and lead to failure.



Physical processes

Fault instability is driven by combination of coupled thermal, hydraulic, mechanical and chemical (THMC) processes, including fluid flow, pressure diffusion, heat transport, mechanical deformation and geochemical reactions. These processes can abruptly upset the balance between fault strength and the applied forces to trigger a seismic event. For example, during hydraulic processes, an increase in fluid pressure could result in changes of effective stress and hence lead to fault reactivation. Moreover, the fluid pressure variations will cause changes in fluid advection that can in turn affect both the temperature and potential chemical reactions.

A detailed understanding of coupled THMC triggering mechanisms must be holistically understood to determine the failure conditions for a pre-existing fault. Unfortunately, the analyses of coupled THMC processes in the subsurface are challenging, both computationally and owing to limited data accessibility. Often, cautious approximations only consider the dominant THMC components and discount the less substantial ones^{132,221,222}. However, the dominant physical processes are principally related to the nature of the anthropogenic forcing, geological setting and in situ conditions.

experiments¹⁰³. Many prominent case histories were explained by earthquake static stress transfer during EGS stimulations^{66,104–106}, hydraulic fracturing^{107,108}, WWD^{109,110} and UGS¹¹¹.

Aseismic slip or reservoir creep. Earthquakes are manifestations of unstable slip, requiring the resistance to sliding diminishes faster than the elastic unloading (creating a force imbalance)¹¹². If this condition is not met, fault displacement is aseismic. Detecting aseismic slip is challenging and has rarely been seen, except in exceptional natural and induced earthquake circumstances^{113,114}. The observed fault displacement during in situ injection experiments on borehole televiewer can be substantially larger than the slip attributed to the largest induced event, implying that most of the fault displacement occurred aseismically¹¹⁵. This has also been confirmed by small-scale injection experiments at relatively shallow depth in underground

laboratories, in which seismo-hydrromechanical responses of fault zones were precisely monitored¹¹⁶.

On critically stressed faults, the aseismic slip front can outpace the pore-pressure front and extend beyond the characteristic length of pressure diffusion¹¹⁷. The conditions over which the aseismic rupture front outpaces the pore-pressure front depend on the stress criticality of the pre-existing faults. The aseismic rupture front can be estimated by the product of the pore-pressure front and a correction factor that is a function of stress criticality. Several studies suggested that aseismic slip was a contributing mechanism to several prominent induced seismicity cases in EGS stimulation^{118,119}, hydraulic fracturing¹¹⁴ and UGS⁵⁰. This can explain the induced earthquakes at distant locations from the injection point.

Aseismic deformation during fluid extraction is typically referred as reservoir creep, which is the inelastic response of rocks. Reservoir

creep or time-dependent viscous deformation is a potential mechanism to impose an additional stress perturbation within the hydrocarbon reservoirs driving further instability. This can be explained by the temporal variation of the differential stressing rate driven by fluid extraction¹²⁰. Reservoir creep explains the discrepancy between the observations and the anticipated deformation computed by poroelasticity theory¹²¹. Moreover, the delay between the pressure depletion and subsidence is often related to time-dependent viscous deformation¹²². These concepts have been proposed to explain the sharp decrease of seismicity rate after the production reductions in the Groningen gas field¹²³.

Fault weakening

Stress corrosion and geochemical interactions. Fluid injection or extraction can change the geochemical equilibrium in the subsurface and expedite fluid–rock interactions. Geochemical processes result in dissolution and/or precipitation of minerals along pre-existing fracture planes and thereby modify the strength of the interface. Stress corrosion often reduces the friction and hence fault strength. In EGS reservoirs, secondary minerals such as clay are formed during hydrothermal alteration and markedly reduce the frictional strength of the rocks. Aseismic slip along such weak zones can substantially perturb the stress field during the injection operations and influence seismicity¹²⁴. In CO₂ storage, the geochemical processes can contribute to stress corrosion and generation of new cracks around faults¹²⁵. However, fault weakening owing to geochemical processes requires longer timescales and could be insubstantial during short-term hydraulic fracturing injections. For instance, Westaway and Burnside¹²⁶ proposed the stress corrosion as a potential triggering mechanism of M_w 5.4 earthquake during hydraulic stimulation of Pohang EGS. They related the delay of 2–3 months between the injection and shock to the time needed for the fluid–rock interactions to take effect.

Dynamic weakening. Earthquakes are generally described as stick–slip phenomenon, in which the dynamic friction is lower than the static value. Slip hardening results in aseismic creep and occurs when the frictional resistance increases with slip. By contrast, slip weakening is the requirement for instability, in which the friction decreases with slip¹¹². Any reduction of the frictional strength promotes further instabilities, and frictional properties of faults have been investigated in many studies dealing with natural earthquakes. Note that the fault-weakening studies were mostly executed in the laboratory conditions. For a detailed review on the dynamic weakening mechanisms of faults, we refer to Di Toro et al.¹²⁷.

Cohesion loss. The strength of rock mass is composed of frictional and cohesive resistances. However, the cohesive strength of faults is commonly disregarded in crustal conditions, as it is small compared with frictional strength^{22,128}. Experiments and observations show that both friction and cohesion increase with time after fault slip¹²⁹. This restrengthening of inactive faults can be sufficiently high to influence the long-term strength. During the co-seismic slip, the cohesion is decreased and this cohesion loss can lead to higher stress drops creating stronger static and dynamic interactions, triggering more events¹³⁰. Despite progress, the mechanisms of cohesion loss and its impact on fault rupture are not sufficiently explored yet.

In general, all mechanisms discussed earlier can contribute to the triggering of seismicity, because induced earthquakes can be triggered by stress changes slightly higher than the stress perturbations caused by the tides of the Earth^{131,132}. However, unravelling the

influence of a single mechanism is challenging. Multiphysical modelling of well-characterized injection and extraction locations shows that the relative significance of triggering mechanisms can vary from site to site depending on the physical rock properties, reservoir structure, operational parameters, fault geometry, seismotectonic conditions and distance from injection and extraction, among others. However, pore-pressure change is considered a primary mechanism for injection-induced seismicity^{21,70,132,133}, and poroelastic coupling is the major mechanism of extraction-induced seismicity⁸⁸.

Maximum induced earthquake magnitude

Despite advances in physical understanding, forecasting the seismic response to industrial activities remains challenging. Frequent changes in operation (such as injection or extraction rates) result in pronounced time-dependent induced earthquake rates. Moreover, seismicity in some regions occurs at a problematic level, whereas other regions remain relatively quiet, even if injection or extraction volumes are comparable¹³⁴. The variability of the seismic response to industrial activity has been related to various natural factors including the regional tectonics, number, size and orientation of pre-existing fractures and faults, local stratigraphy and existence of hydraulic conduits^{19,135}.

Forecasting the number and magnitude of earthquakes that might be induced during the lifetime of a project has a critical role in the assessment of the seismic hazard and risk. Ultimately, the seismic risk associated with induced seismicity depends on whether a large magnitude earthquake is triggered¹³⁶. In some cases, damaging magnitude thresholds have been exceeded and substantial economic losses and even several fatalities have been reported^{68,137}. However, understanding and forecasting the maximum magnitude induced by industrial activity is problematic, because models for single events M_{\max} are inherently associated with large uncertainty. To date, it is unclear whether M_{\max} can be meaningfully forecasted on the basis of physical and statistical principles.

From a statistical view, maximum observed induced earthquake magnitude in many cases agrees with the modal value of M_{\max} expected from the Gutenberg–Richter relation¹³⁸:

$$M_{\max} = M_c + \frac{1}{b} \log(N), \quad (1)$$

in which M_c is the magnitude of completeness, N is the number of events larger than or equal to M_c and b is the b -value estimated from the observed earthquake magnitudes. Overall, reported b -values of induced earthquake sequences are close to $b = 1$, in agreement with b -values of tectonic earthquakes. However, b -values in the range of 0.5–3.0 and time-dependent b -values have been discussed^{139,140}. Equation (1) implies that there is no upper limit to the maximum possible magnitude. The more earthquakes above M_c that occur, the larger the M_{\max} is expected to be. Note that equation (1) is based on observations and cannot be directly used to forecast the expected maximum magnitude before or during operation. To allow forecasts of M_{\max} , it should be combined with physics-based seismicity models estimating the expected number of events larger than or equal to M_c .

Volume-based theories

The seismogenic index theory¹³⁴, in which pore-pressure diffusion is the dominant triggering mechanism, incorporates the injected fluid volume to forecast the number of events $\geq M$ according to equation (2):

$$\log N_M(t) = \Sigma + \log V(t) - bM, \quad (2)$$

in which $N_M(t)$ is the number of magnitudes larger than or equal to M , b is the b -value, $V(t)$ is the cumulative injected fluid volume (in m^3) and Σ is the seismogenic index. Σ is a time-independent site-specific property describing the susceptibility to induced earthquakes. Reported Σ values are between -10 and 1 (ref. 141). The seismogenic index incorporates all unknown site-specific seismo-tectonic parameters and can be calibrated using observed magnitudes and reported injection volumes. Combination of equations (1) and (2) can be applied to estimate the expected maximum magnitude according to¹³⁸:

$$M_{\max} = \frac{1}{b} [\Sigma + \log(V)]. \quad (3)$$

The higher the seismogenic index, the larger the expected maximum magnitude for a given injection volume. The seismogenic index model was originally developed for EGS and hydraulic fracturing experiments with single injection boreholes¹⁴², but has been extended to field-scale injection settings^{63,143}, to include a hydrogeological model⁶¹, poroelastic effects, extraction-induced seismicity¹⁴¹ and arbitrary physical processes causing Coulomb stress perturbations¹⁴⁴.

Generally, the validity of Gutenberg–Richter relation is accepted in all existing M_{\max} models. The main point of discussion is whether an overall or time-dependent limit to the maximum possible induced magnitude exists. When a critically stressed fault ruptures owing to a perturbation by fluid injection or production, it releases the stored tectonic strain energy. In this case, the rupture can extend beyond the pressure front and M_{\max} is largely controlled by the dimensions of the largest fault reactivated by anthropogenic activities. This viewpoint is supported by the focal mechanisms of larger magnitude events induced by hydraulic fracturing, WWDs and EGS stimulations, which correspond to failure of optimally oriented faults in the tectonic stress field^{136,145}.

In this direction, using a geometrical approach, injection-induced earthquakes mainly occur along faults located inside the stimulated rock volume¹⁴⁶. The finding suggested that the maximum possible magnitude gets larger with time as the perturbed rock volume grows. The main factor limiting the probability to induce a larger-magnitude event is the minimum principal axis of the fluid-stimulated rock volume. Shapiro et al.¹⁴⁶ extended the geometrical approach to more complex perturbed rock volumes and faults only partially located inside the stimulated zone. A similar approach was also adopted to constrain the largest rupture plane in a cuboid perturbed volume using discrete fracture network models¹⁴⁷.

McGarr¹⁴⁸ proposed an empirical relation between M_{\max} and injected volume, which defines an upper bound to the released seismic moment as in equation (4):

$$M_0 = GV, \quad (4)$$

in which M_0 is the cumulative seismic moment, G is the shear modulus (approximately 30 GPa) and V is the cumulative injected volume. McGarr's model can be used to estimate M_{\max} before injection operations. However, observations of large magnitude events of fluid injections^{36,149} exceeded M_{\max} of McGarr's model. McGarr's model was also reformulated by adding a term representing the initial stress state on a fault, which explained the M_{\max} in several case histories¹³. More complex volume-based models were developed incorporating rupture physics¹⁵⁰. The model considered two rupture modes of self-arrested and runaway ruptures, and the transition between these modes is

controlled by the area and the amplitude of the pressure front, friction parameters and the stress state. However, the nucleation and arrest of a dynamic slip could be linked to the injection rate ramp-up, with larger slip associated with slower injection ramp-up when the fault is not critically stressed¹⁵¹.

Time-based theory

The case histories of induced earthquakes were used to show that M_{\max} scales with the logarithm of nucleation time¹⁴ (that is, the elapsed time from the beginning of the fluid injection) (Fig. 3). They also argued that the earthquake triggering time better describes observed maximum magnitudes compared with scaling with injected volume and proposed the following:

$$M_{\max} = 2\xi \log(T) + \text{const.} \quad (5)$$

in which ξ accounts for the physical mechanism and T is the triggering time ($\xi = 0.5$ in the case of pore-pressure diffusion). The proposed time-based M_{\max} model successfully explained the magnitude and nucleation time of runaway ruptures such as the 2017 Pohang earthquake. Runaway ruptures account for the case in which the triggering seismicity front outpaces the perturbed volume. However, current application of this model is limited to real-time monitoring of seismotectonic properties of the target reservoir such as seismogenic index. Langenbruch et al.¹⁵² further elaborated on the scaling of M_{\max} with time and discussed the increasing nucleation potential of larger magnitude earthquakes with time based on diffusion-controlled growth of pressure-perturbed fault sizes.

To date, there is no standard or best practice of how methods of the maximum possible induced earthquake magnitude are applied. Basically, the maximum possible induced magnitude should be estimated pre-operation based on an ensemble of existing methods. The range of estimated maximum magnitudes should be used to perform pre-operation scenario loss modelling to understand whether a planned project is within the local risk tolerance^{12,136}. In any case, uncertainty must be considered when assessing the maximum magnitude. The wide probability distribution of the maximum magnitude makes it impractical to base decisions about continuation, modification or termination of an energy project on the expected or observed maximum magnitude. The seismic risk posed by the occurrence of low-probability, large-magnitude events can be high but unidentified¹³⁶. Forward-looking probabilistic approaches^{14,61,80,86,153,154} should be applied in real-time to update the assessments of the maximum induced earthquake magnitude, seismic hazard and risk.

In general, the observed M_{\max} of documented past events revealed the absence of an upper deterministic limit. If a critically stressed fault is somewhat perturbed by fluid injection or production, the amount of tectonic strain energy controls the extent of rupture, which could be far beyond the pressure front. In such cases, the M_{\max} can be as large as that of natural earthquakes¹⁵⁵.

Monitoring, discrimination, risk, hazard and mitigation

The concepts of monitoring, discrimination, risk, hazard and mitigation are important to managing induced seismicity as they provide the means to quantify possible losses and to identify actions that can reduce the severity and frequency of these losses. In this section, these concepts are discussed with respect to the underlying physical mechanisms.

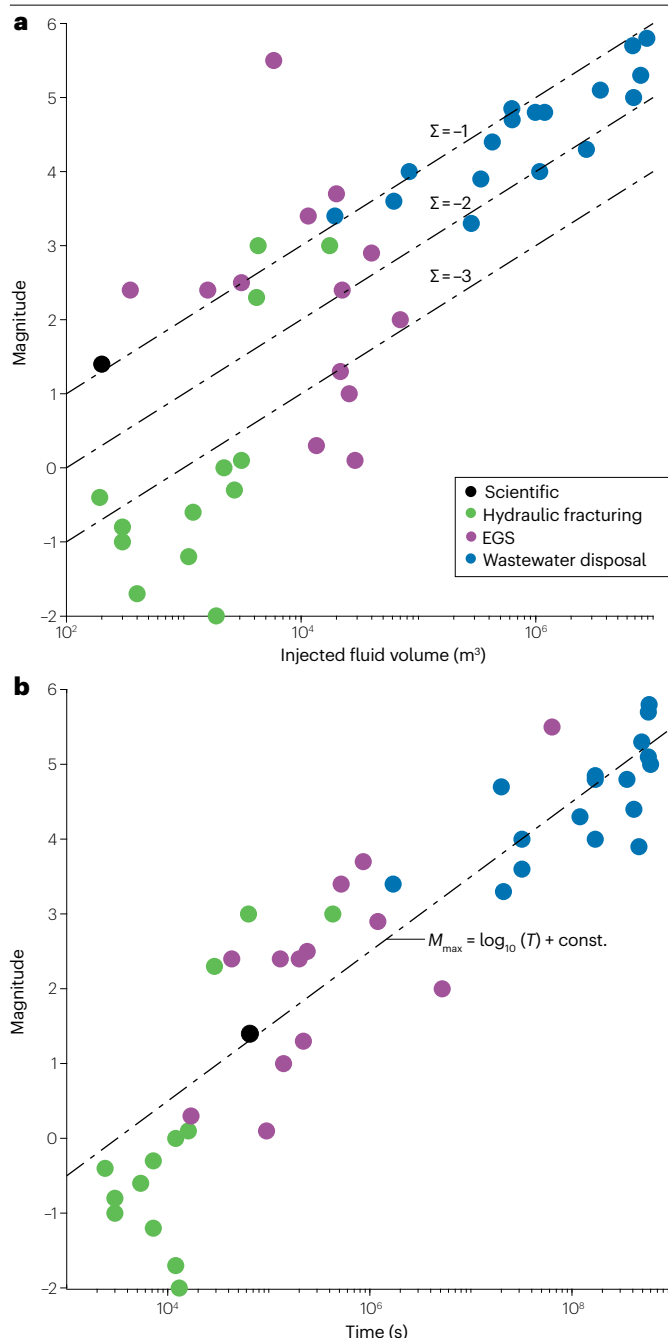


Fig. 3 | Calculating maximum magnitudes of induced earthquakes. Each data point corresponds to the maximum magnitude observed for 44 specific events of hydraulic fracturing, enhanced geothermal system (EGS) stimulation, water disposal and injection at scientific boreholes. **a**, M_{\max} data plotted against the injected fluid volume. The dashed lines show the seismicogenic index model^{14,138} for seismicogenic index values of $\Sigma = -3$, -2 and -1 and $b = 1$. **b**, Maximum magnitude data plotted against the time from start of fluid injection until occurrence of the earthquake. The dashed solid line shows the proposed scaling of the maximum magnitude with the logarithm of the time with $\xi = 0.5$. Figure adapted from ref. 14 under a Creative Commons licence CC BY 4.0.

monitoring is essential to support the best risk mitigation strategies¹⁵⁸. The design of a seismic network is often performed following empirical, sometimes subjective, considerations without taking into account the type of industrial activity being monitored¹⁶. Thus, advanced physical models for the simulation of the stress perturbation caused by a particular industrial operation and the simulation of associated induced seismicity can be used to evaluate (at least as a first-order approximation) the extent of the area requiring monitoring and the characteristics (in terms of magnitude and spatial distribution) of the target seismicity. In other words, physical modelling of induced seismicity can provide information on the minimum magnitude that should be detected and on the required location accuracy that should be reached by the monitoring infrastructure, giving objective constraints on design parameters of different seismic networks such as the aperture of the network (that is, the spatial extension), the number and the location of the seismic stations.

Physics-based models are also extremely important in the discrimination between natural and induced seismicity, a challenging problem that is not yet resolved. To date, no physical difference between the mechanism of natural and anthropogenic earthquakes has been found. It seems likely that they are not. Discrimination of induced seismicity is often performed, in a rather qualitative way, by considering the spatial and temporal 'closeness' (which is per se subjective) between the seismicity and the industrial operations^{159,160}. Although spatial and temporal correlation between human industrial operations and seismic events might represent a first-order approximation to discriminate between natural and anthropogenic seismicity¹⁶, a causal link can only be found using physical modelling approaches. Without a detailed study involving seismicity analysis, pore-pressure diffusion¹⁴², poroelastic stress modelling and an assessment of the geological setting of the area⁶⁶, the discrimination between natural and induced seismicity is uncertain or even impossible. Physics-based models combined with seismicity models, such as rate-and-state seismicity models¹⁰², allow simulation of the evolution of seismicity in the space–time–magnitude domain. Furthermore, contemporaneous operations can each contribute to reactivating a fault^{45,161}, providing cases in which determining a single causal factor becomes complicated (or even impossible). By comparing simulated seismicity with the real one, it is, in principle, possible to answer the question regarding the origin and relative contributions of suspected cases of induced seismicity by directly investigating the physical processes governing such phenomenon (that is, stress perturbations caused by each of the industrial operations).

Seismic hazard and risk assessment

Within the scope of natural tectonic seismicity, the use of probabilistic seismic hazard analysis (PSHA) is the de facto approach to

Monitoring and discrimination

Microseismic monitoring operations can have a crucial role to ensure the safety of underground industrial operations within real-time-induced seismicity risk management procedures¹⁵⁶. The optimal design of a microseismic monitoring network allows for improved detection and location performance for natural and induced microseismicity as well as the estimation of magnitudes¹⁵⁷ and other source parameters¹⁶. In this context, a better understanding of the physical mechanisms governing induced seismicity, hence an improved capability to simulate synthetic-induced seismicity catalogues, can greatly help to optimize network design before industrial operations begin. Pre-operational

understanding hazards from earthquake ground shaking¹⁶². For example, PSHA-derived hazard curves inform building design codes, insurance policies and earthquake disaster reaction policies. The PSHA workflow constitutes three components: source modelling, ground motion characterization and hazard curve estimation – these procedures are inherently statistical, owing to the unpredictable nature of earthquakes. Unfortunately, the nature of induced seismicity poses additional problems for the traditional PSHA source modelling assumptions, as induced seismicity rates are not stationary on human or construction time frames. Initial attempts to characterize induced earthquake hazards sidestepped this stationarity problem by instead producing a series of short-time assessments¹⁶³. Thus, future efforts that enable forecasting^{17,158} would allow for more complete hazard assessments, in which physics-based models can provide alternatives to statistics-based approaches.

Currently used M_{\max} theories made simplifying assumptions in characterizing earthquake sources, owing to the difficulty and variability in observing relevant in situ properties; for example, by considering injected volume as a proxy variable to anticipate seismic response (such as event counts or seismic moment)^{134,148,150}. These models have provided suggestions towards potential magnitude upper bounds¹³⁸ and the seismogenic potential of reservoirs¹⁶⁴. The simplicity of these models has hampered their ability to account for delayed seismic responses, trailing seismicity (earthquakes that continue to occur after well shut-in), the Kaiser effect (a hysteresis in which events often occur only after exceeding previous stress extremums), or non-direct pore-pressure effects (such as poroelastic stress changes). Because of these limitations, modifications have been suggested that consider new maximums in Coulomb stress changes¹⁴⁴, addition of exponential tails following shut-in^{158,165} or convolution with Omori-like rate decay functions¹⁶⁶. More physically motivated models have also been suggested that are based on empirical frictional relations and stress rate changes that can account for stress-delayed seismic response and trailing seismicity¹⁶⁷. More sophisticated, still hydromechanical models have been used to model seismic rates at secondary oil fields¹⁶⁸ and gas fields¹⁶⁹. In some cases, hybrid statistical–geomechanical

approaches have been used for spatiotemporal seismic forecasting¹⁷⁰. Also, machine-learning approaches have attempted improved forecasting^{171–173}, especially given the success in the laboratory settings¹⁷⁴. In some studies, machine-learning techniques have been used towards better understanding of the relative importance of input variables for the forecasting of seismic response^{172,175}. The proliferation of these forecast models has also raised questions about discerning the suitability of approaches; here, ensembles of models can be aggregated on the basis of their relative data fit¹⁷⁶, with composite forecasts often outperforming any individual model¹⁷⁷.

To manage induced earthquake risks, a TLP is often adopted¹⁷⁸. A TLP typically defines the green light as the threshold that allows unrestricted operations to proceed, the yellow light as the threshold to initiate mitigation strategies and the red light as the point requiring a regulatory intervention (including a cessation of the causal operation). Work has also begun to tie the design of TLPs to risk-based metrics including nuisance, building damage and chance of fatality¹⁷⁹ as well as to adapt them to real-time information¹⁸⁰. Characterizing the events that can trail the end of an operation^{181,182} will be particularly important, as they are the most influential parameters under typical risk management¹².

However, these approaches rely on a statistical estimation of the events that trail the end of an operation. The use of physics-based models has a potential role in modelling and forecasting the expected seismicity, to anticipate future hazard and risk and feedback information for operational adjustments or mitigation (Fig. 4).

Mitigation strategies

In the context of a TLP, the success of an operator strongly depends on the efficacy of mitigation strategies applied at the yellow-light level. In an ideal case, mitigation strategies would effectively reduce seismic risks and hazards, to ultimately avoid the operation-ending red-light scenario. Here, mitigation strategies are broadly defined as approaches that aim to decrease the hazards of induced seismicity. Mitigation strategies involve either reactionary approaches or longer-term avoidance or planning approaches. Traditionally, the reactionary strategies have

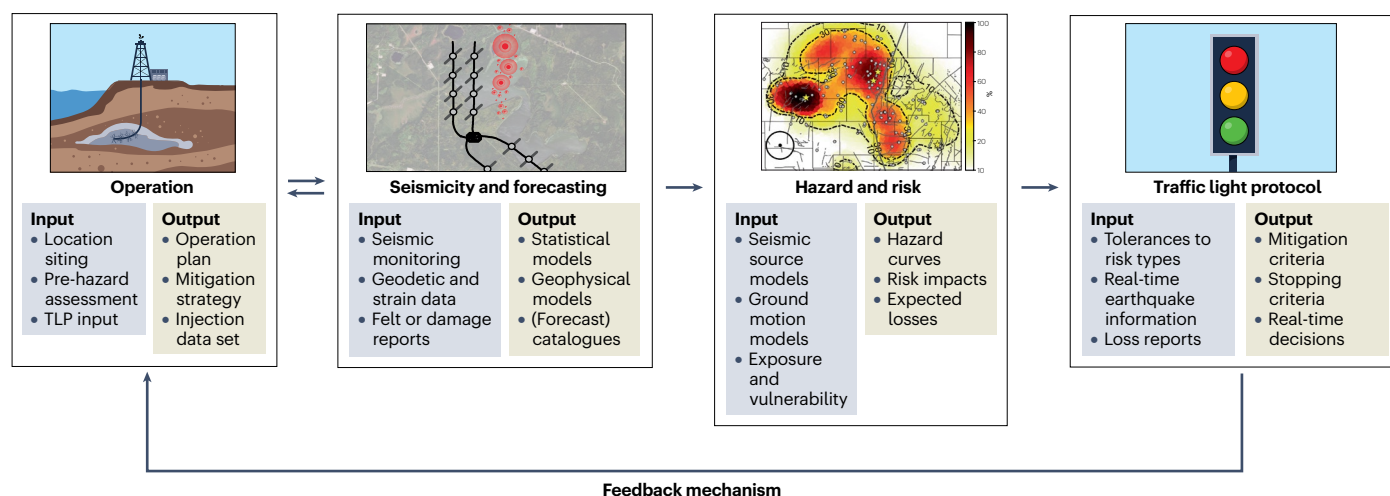


Fig. 4 | The operation and induced seismicity feedback loop. Operations are planned to avoid and minimize the impacts of induced seismicity. Seismic and geophysical monitoring provide data for models that can forecast earthquakes. Earthquake catalogues and source models can be used in hazard and risk

assessments. Finally, risk and hazard assessments can be used to inform the design of a traffic light protocol (TLP), which acts as a real-time decision module for the operation. Each panel shows the categories of input information (blue boxes) and output products (orange boxes).

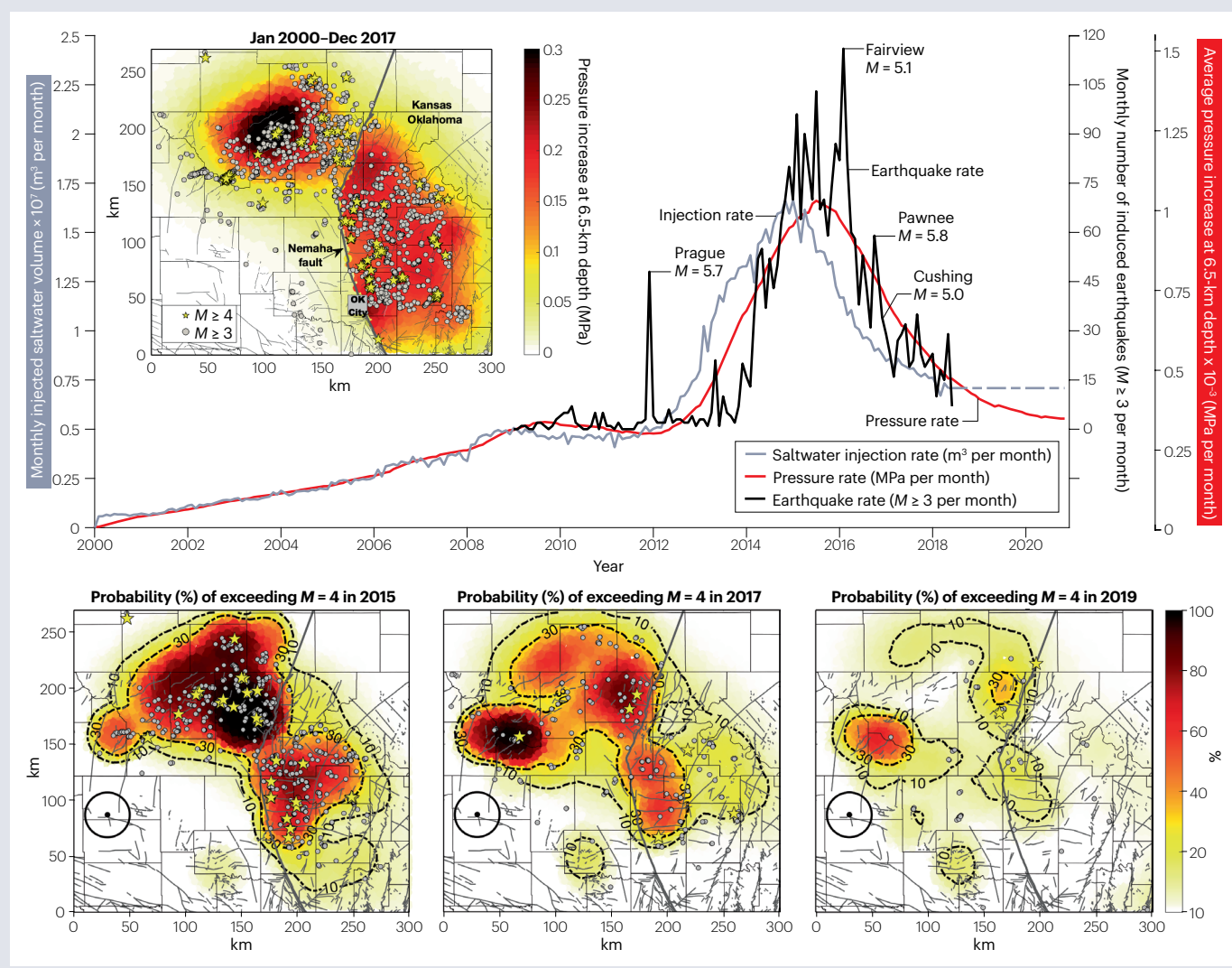
Box 2

Oklahoma case study

A marked increase in seismic activity occurred in the Central and Eastern USA in 2009, predominantly in north-central Oklahoma and southernmost Kansas (see the figure, black line, top panel). Many of the oil wells in Oklahoma and Kansas produce more water than for oil. Because the produced water is too saline and contaminated to be put to beneficial use, it is disposed into the deepest sedimentary formation, called the Arbuckle group. Since 2014, the region has experienced thousands of widely felt earthquakes ($M \geq 3$) caused by the deep injection of this contaminated salt water (grey line)^{61,63,223} (see the figure, top plot). To date, three earthquakes exceeded $M = 5$, including the September 2016 Pawnee $M = 5.8$ earthquake — the largest in instrumented history in Oklahoma and Kansas. In comparison, hydraulic fracturing has caused less widely felt earthquakes than those from wastewater disposal in Oklahoma⁷⁰.

The Arbuckle group is in hydraulic communication with faults in the crystalline basement, where natural geological processes have accumulated stress on pre-existing faults. The increase in pressure resulting from saltwater injection is propagating away from the injection wells and down into the crystalline basement. Where the pressure increase finds critically stressed faults, earthquakes are triggered.

The seismic activity in north-central Oklahoma and southernmost Kansas peaked in 2015, when 943 widely felt $M \geq 3$ ($31M \geq 4$) earthquakes occurred in response to the increase in produced water injection. Earthquakes (inset map; $M \geq 3$ grey dots, $M \geq 4$ yellow stars) generally occurred in regions in which injection-induced pressure increased at depth (red–yellow colouring; calculated from a physics-based model, between Jan 2000 and Dec 2017). Injection volumes then started to decrease rapidly in mid-2015, driven by market forces (a drop in oil



(continued from previous page)

price in late 2014) and mandated large-scale volume reductions. The earthquake rate responded to decreased injection rates and reduced by about 97% through 2021. In 2021, 33 M3+ (1 M4+) earthquakes were recorded. Currently, the seismicity in the region occurs at rates similar to those observed in 2009–2013. Although the overall earthquake rate has decreased markedly since mid-2015, the anthropogenic seismic hazard is still higher than the natural tectonic earthquake hazard of about one M3+ earthquake per year.

A physics-based model was developed on the basis of the understanding of pressure diffusion as the triggering mechanism

of induced earthquakes in Oklahoma and Kansas⁶¹ (see the figure, lower plots; representing 1-year forecasts to exceed M4 in regions of 20-km radius). In the model, seismicity is driven by the rate of injection-induced pressure increases at any given location, and spatial variations in both the number and stress state of pre-existing basement faults affected by the pressure increase. The observed temporal and spatial decline of the seismic hazard in Oklahoma and Kansas since mid-2015 was successfully forecast using this method (see the figure, lower plots).

Figure adapted from ref. 61 under a Creative Commons licence CC BY 4.0.

entailed approaches including rate, pressure and/or volume reduction, operation pausing, skipping and even abandonment as a last resort. Avoidance or planning approaches entail monitoring, stress measurement, geophysical hazard pre-assessments and injection or production design¹⁹. In this sense, physics-based models could provide notable improvements via suggesting and testing approaches to mitigation.

Physics-based principles have suggested several mitigation strategies throughout the history of induced seismicity. For example, one physically informed mitigation strategy is the slow change of injection or production rates to their targets (rather than sudden, step-like changes). This idea is rooted in concepts derived from both friction laws (that anticipate dynamic slip conditions from sudden rate changes¹⁸³) and water hammer effects (dynamic pressure pulses from suddenly driving a rate change¹⁸⁴). Empirically, this rate-change effect has often been sporadically supported through anecdotal examples at the field scale¹⁸⁵ and in the laboratory¹⁸⁶. In another example, the observation-driven compaction model at Groningen¹⁶⁹ led the re-prioritization of gas production: focusing the greatest extraction from wells at the margins of the field (where compaction was less pronounced) to relieve compaction from central wells (where seismic response was greatest)⁵⁴. Although this rationale is conceptually sound, these changes were unfortunately unable to prevent the abandonment of this gas field¹⁸⁷. Additionally, physics-based principles have suggested strategies such as fracture caging¹⁸⁸, cyclic stimulation¹⁸⁹, injection schemes that promote aseismic slip¹⁸⁶ and even injection schemes that attempt to control and stabilize fault slip^{190,191}. The continued suggestion and evaluation of mitigation strategies from physical principles will allow for their refinement.

However, evaluating the effectiveness of mitigation strategies has largely been restricted by the availability of data. Field-scale data sets required to better understand the underlying processes include high-resolution earthquake catalogues along with injection time-series data, for a wide variety of cases, operations and settings^{7,192,193}. Building upon this, either in situ strain measurements or geodetic observations can be particularly helpful for partitioning aseismic and seismic fault moment release^{194,195}. To date, progress on mitigation during the active stages of injection has been restricted to inference from laboratory analogues or via decametre-scale experiments within tunnels or mines⁷. There have been some cases in which field-scale physical models have been developed^{168,196}. Given the paramount importance of mitigation strategies for reducing seismic hazards and risks, high-resolution data sets and experiments will be required to validate their efficacy and build best practices at the field scale.

As an example, seismicity induced by WWD presents additional challenges, as the connection between the source (injection wells) and the response cannot be determined in many cases owing to the large number of wells, the large distances between them and the fabric, such as faults and fractures in the injection strata, which can exert strong directional control on the induced earthquakes. It can also lag injection by many months. This time lag makes physical sense and corresponds to the time the pressure and stress changes need to propagate from the injection wells to the pre-existing critically stressed faults. It is controlled by factors such as the distance between injection intervals and pre-existing faults, hydrogeological conditions, as well as the stress changes needed for fault reactivation. Examples in Alberta, Canada, suggest that seismicity can lag the operation of WWD by years or even decades^{45,197–199}.

The time lag was particularly evident during the seismic crisis in Oklahoma case (Box 2) in 2014–2016 when the state government acted to substantially reduce WWD volumes in mid-2016⁶³. By reducing, but not stopping disposal, seismicity has stabilized, although it remains elevated relative to the tectonic background rate⁶¹. Similar steps have been taken in TX, USA in response to elevated seismicity near the cities of Midland and Odessa since 2022. Time will tell whether these reductions prove sufficient or whether other measures must be taken²⁰⁰. Geomechanical approaches for managing WWD over the long term appear promising, based on the understanding gained from induced seismicity in the Oklahoma case²⁰¹.

In summary, physics-based approaches can enhance the current seismic monitoring, hazard and risk assessments and mitigation strategies. However, even the state-of-the-art cannot anticipate and prevent the occurrence of moderate-to-large magnitude earthquakes, namely, exceeding M4.

Summary and future directions

Underground fluid injection and extraction activate complex physical processes that destabilize pre-existing faults. Fluid-induced earthquakes are mainly triggered by in situ stress perturbations on critically stressed faults. However, human activities might reactivate faults that were not critically stressed before the start of operation. The major triggering mechanisms of injection-induced and extraction-induced seismicity are pore-pressure diffusion and poroelastic coupling, respectively. During injection, pore-pressure elevation reduces the effective normal stress acting on fault planes leading to failure. Also, poroelastic coupling can lead to reservoir compaction and perturb the stress field in the surrounding rock formations during fluid extraction and trigger earthquakes. These mechanisms often explain most seismic swarms

around injection or extraction sites. However, other mechanisms such as aseismic deformation and earthquake interactions explain the stress transfer to distant locations.

Multiphysical modelling studies at well-characterized locations show that the relative importance of different triggering mechanisms can vary from site to site. An important aspect is the complex interaction among different industrial activities specifically when the earthquakes occur in an area where both hydraulic fracturing and WWD are occurring. One important question is to determine the dominating mechanisms and the main activity that is responsible to generate each seismicity cluster²⁰². Apparently, the amount of stress perturbation caused by different activities can be highly nonlinear and depends on many physical factors such as the distance to each well, the amount of injected volume, the operational time windows and the corresponding geological and hydrological characteristics¹⁶¹.

Also, debates on the triggering mechanism or hypocentral depth of induced earthquakes are typically related to poor monitoring infrastructure such as in offshore operations^{161,203,204}. Hence, physics-based design of microseismic monitoring network at each site might aid inferring the controlling mechanisms of induced seismicity. As an alternative, distributed acoustic sensing technology, which utilizes an optical fibre cable as the sensing element, can be sensitive enough to record microseismic events and provide reliable depth estimations²⁰⁵. However, further research is necessary to elucidate the complementary opportunities and inherent limitations of distributed acoustic sensing technology²⁰⁶.

The current physical understanding is often inferred from large-scale in situ experiments, in which the limited access and exposure of the target rock mass at great depth hinders precise measurements of THMC changes in the rock mass. As an alternative, in situ experiments at underground laboratories (decametre-to-hectometre scale) are evolving as an alternative to bridge the gap between the observations in the laboratory²⁰⁷ and field-scale operations. The major advantage of small-scale experiments is the possibility to precisely characterize the rock mass and in situ condition with full control over operational variants. Extensive instrumentation provides high-resolution data sets that determine the physical processes controlling the seismicity and test the effectiveness of methodological advances that mitigate the seismic risk²⁰⁸. In addition, such experiments can benchmark the numerical models that resolve the coupled processes at in situ conditions^{8,209}. However, numerical modelling of coupled processes demands an intensive computational effort. Hence, the developments in high-performance and efficient computing tools such as physics-based machine learning open a new door to resolve the 3D multiphysics problems and to quantify the uncertainty of the model parameters²¹⁰.

Ideally, the evaluation of induced seismicity hazard should be conducted with a deterministic approach, with high-resolution characterization of pre-existing fractures and faults²¹¹, detailed 3D stress information²¹², a fundamental understanding of physical mechanisms and transparent injection plans. In reality, these priors are barely available and constraining the magnitude and triggering time of induced earthquakes is challenging, just like natural earthquakes. Therefore, at the current stage, induced seismicity hazard has to be estimated statistically and only a few physical factors are integrated into physics-based models. From this aspect, our Review elucidates the importance of physics-based models that capture the multiphysical processes that control the rupture nucleation, propagation and arrest across multiple regions and scales.

Published online: 5 December 2023

References

- Kim, K.-H. et al. Assessing whether the 2017 M_w 5.4 Pohang earthquake in South Korea was an induced event. *Science* **360**, 1007–1009 (2018).
- Zöller, G. & Hainzl, S. Seismicity scenarios for the remaining operating period of the gas field in Groningen, Netherlands. *Seismol. Res. Lett.* **94**, 805–812 (2023).
- Lengliné, O. et al. The largest induced earthquakes during the GEOVEN deep geothermal project, Strasbourg, 2018–2022: from source parameters to intensity maps. *Geophys. J. Int.* **234**, 2445–2457 (2023).
- Foulger, G. R., Wilson, M. P., Gluyas, J. G., Julian, B. R. & Davies, R. J. Global review of human-induced earthquakes. *Earth Sci. Rev.* **178**, 438–514 (2018).
- Evans, Z. A., Kraft, T., Deichmann, N. & Moia, F. A survey of the induced seismic responses to fluid injection in geothermal and CO₂ reservoirs in Europe. *Geothermics* **41**, 30–54 (2012).
- McGarr, A., Simpson, D., Seeber, L. & Lee, W. Case histories of induced and triggered seismicity. *Int. Geophys. Ser.* **81**, 647–664 (2002).
- Amann, F. et al. The seismo-hydro-mechanical behaviour during deep geothermal reservoir stimulations: open question tackled in a decameter-scale in-situ stimulation experiment. *Solid Earth Discuss.* **2017**, se-2017-se-2079 (2017).
- Gischig, V. S. et al. Hydraulic stimulation and fluid circulation experiments in underground laboratories: stepping up the scale towards engineered geothermal systems. *Geomech. Energy Environ.* **24**, 100175 (2019).
- Kneafsey, T. J. et al. in *Proceedings of the 45th Workshop on Geothermal Reservoir Engineering* 10–12 (Stanford, CA, USA, 2019).
- Zang, A. et al. How to reduce fluid-injection-induced seismicity. *Rock Mech. Rock Eng.* **52**, 475–493 (2019).
- Kwiatk, G. et al. Controlling fluid-induced seismicity during a 6.1-km-deep geothermal stimulation in Finland. *Sci. Adv.* **5**, eaav7224 (2019).
- Schultz, R., Beroza, G. C. & Ellsworth, W. L. A risk-based approach for managing hydraulic fracturing-induced seismicity. *Science* **372**, 504–507 (2021).
- Li, Z. et al. Constraining maximum event magnitude during injection-triggered seismicity. *Nat. Commun.* **12**, 1528 (2021).
- Shapiro, S. A., Kim, K.-H. & Ree, J.-H. Magnitude and nucleation time of the 2017 Pohang Earthquake point to its predictable artificial triggering. *Nat. Commun.* **12**, 6397 (2021).
- Li, L. et al. A review of the current status of induced seismicity monitoring for hydraulic fracturing in unconventional tight oil and gas reservoirs. *Fuel* **242**, 195–210 (2019).
- Grigoli, F. et al. Current challenges in monitoring, discrimination, and management of induced seismicity related to underground industrial activities: a European perspective. *Rev. Geophys.* **55**, 310–340 (2017).
- Gaucher, E. et al. Induced seismicity in geothermal reservoirs: a review of forecasting approaches. *Renew. Sustain. Energy Rev.* **52**, 1473–1490 (2015).
- Atkinson, G. M., Eaton, D. W. & Igonin, N. Developments in understanding seismicity triggered by hydraulic fracturing. *Nat. Rev. Earth Environ.* **1**, 264–277 (2020).
- Schultz, R. et al. Hydraulic fracturing-induced seismicity. *Rev. Geophys.* **58**, e2019RG000695 (2020).
- Suckale, J. Moderate-to-large seismicity induced by hydrocarbon production. *Lead. Edge* **29**, 310–319 (2010).
- Keranen, K. M. & Weingarten, M. Induced seismicity. *Ann. Rev. Earth Planet. Sci.* **46**, 149–174 (2018).
- Ellsworth, W. L. Injection-induced earthquakes. *Science* **341**, 1225942 (2013).
- Rathnaweera, T. D., Wu, W., Ji, Y. & Gamage, R. P. Understanding injection-induced seismicity in enhanced geothermal systems: from the coupled thermo-hydro-mechanical-chemical process to anthropogenic earthquake prediction. *Earth Sci. Rev.* **205**, 103182 (2020).
- Zang, A. et al. Analysis of induced seismicity in geothermal reservoirs — an overview. *Geothermics* **52**, 6–21 (2014).
- Li, T., Cai, M. & Cai, M. A review of mining-induced seismicity in China. *Int. J. Rock Mech. Min. Sci.* **44**, 1149–1171 (2007).
- White, J. A. & Foxall, W. Assessing induced seismicity risk at CO₂ storage projects: recent progress and remaining challenges. *Int. J. Greenh. Gas Control* **49**, 413–424 (2016).
- Rutqvist, J. et al. Fault activation and induced seismicity in geological carbon storage — lessons learned from recent modeling studies. *J. Rock Mech. Geotech. Eng.* **8**, 789–804 (2016).
- Grigoli, F. et al. The November 2017 Mw 5.5 Pohang earthquake: a possible case of induced seismicity in South Korea. *Science* **360**, 1003–1006 (2018).
- Häring, M. O., Schanz, U., Ladner, F. & Dyer, B. C. Characterisation of the Basel 1 enhanced geothermal system. *Geothermics* **37**, 469–495 (2008).
- Schmittbuhl, J. et al. Induced and triggered seismicity below the city of Strasbourg, France from November 2019 to January 2021. *Comptes Rendus Géosci.* **353**, 561–584 (2021).
- Barton, N. A review of mechanical over-closure and thermal over-closure of rock joints: potential consequences for coupled modelling of nuclear waste disposal and geothermal energy development. *Tunn. Undergr. Space Technol.* **99**, 103379 (2020).
- Zoback, M. D., Kohli, A., Das, I. & McClure, M. in *SPE Americas Unconventional Resources Conference* (OnePetro, 2017).
- Eaton, D. W. *Passive Seismic Monitoring of Induced Seismicity: Fundamental Principles and Application to Energy Technologies* (Cambridge Univ. Press, 2018).
- Bao, X. & Eaton, D. W. Fault activation by hydraulic fracturing in western Canada. *Science* **354**, 1406–1409 (2016).

35. Schultz, R. & Wang, R. Newly emerging cases of hydraulic fracturing induced seismicity in the Duvernay East Shale Basin. *Tectonophysics* **779**, 228393 (2020).
36. Atkinson, G. M. et al. Hydraulic fracturing and seismicity in the Western Canada Sedimentary Basin. *Seismol. Res. Lett.* **87**, 631–647 (2016).
37. Brudzinski, M. R. & Kozłowska, M. Seismicity induced by hydraulic fracturing and wastewater disposal in the Appalachian Basin, USA: a review. *Acta Geophys.* **67**, 351–364 (2019).
38. Schultz, R., Atkinson, G., Eaton, D. W., Gu, Y. J. & Kao, H. Hydraulic fracturing volume is associated with induced earthquake productivity in the Duvernay play. *Science* **359**, 304–308 (2018).
39. Galloway, E., Hauck, T., Corlett, H., Pană, D. & Schultz, R. Faults and associated karst collapse suggest conduits for fluid flow that influence hydraulic fracturing-induced seismicity. *Proc. Natl Acad. Sci. USA* **115**, E10003–E10012 (2018).
40. Pawley, S. et al. The geological susceptibility of induced earthquakes in the Duvernay play. *Geophys. Res. Lett.* **45**, 1786–1793 (2018).
41. Zhao, Y. et al. The 2021 M_w 6.0 Luxian (China) earthquake: blind reverse-fault rupture in deep sedimentary formations likely induced by pressure perturbation from hydraulic fracturing. *Geophys. Res. Lett.* **50**, e2023GL103209 (2023).
42. Meng, L., McGarr, A., Zhou, L. & Zang, Y. An investigation of seismicity induced by hydraulic fracturing in the Sichuan Basin of China based on data from a temporary seismic network. *Bull. Seismol. Soc. Am.* **109**, 348–357 (2019).
43. Wang, B. et al. A study on the largest hydraulic fracturing induced earthquake in Canada: numerical modeling and triggering mechanism. *Bull. Seismol. Soc. Am.* **111**, 1392–1404 (2021).
44. Pollyea, R. M. et al. A new perspective on the hydraulics of oilfield wastewater disposal: how PTX conditions affect fluid pressure transients that cause earthquakes. *Energy Environ. Sci.* **13**, 3014–3031 (2020).
45. Schultz, R. et al. Disposal from in situ bitumen recovery induced the ML 5.6 Peace River earthquake. *Geophys. Res. Lett.* **50**, e2023GL102940 (2023).
46. Tung, S., Zhai, G. & Shirzaei, M. Potential link between 2020 Mentone, West Texas M5 earthquake and nearby wastewater injection: implications for aquifer mechanical properties. *Geophys. Res. Lett.* **48**(3), e2020GL090551 (2020).
47. Keranen, K. M., Savage, H. M., Abers, G. A. & Cochran, E. S. Potentially induced earthquakes in Oklahoma, USA: links between wastewater injection and the 2011 Mw 5.7 earthquake sequence. *Geology* **41**, 699–702 (2013).
48. Yeck, W. L. et al. Oklahoma experiences largest earthquake during ongoing regional wastewater injection hazard mitigation efforts. *Geophys. Res. Lett.* **44**, 711–717 (2017).
49. Cesca, S. et al. Seismicity at the castor gas reservoir driven by pore pressure diffusion and asperities loading. *Nat. Commun.* **12**, 4783 (2021).
50. Villarrasa, V., De Simone, S., Carrera, J. & Villaseñor, A. Unravelling the causes of the seismicity induced by underground gas storage at Castor, Spain. *Geophys. Res. Lett.* **48**(7), e2020GL092038 (2021).
51. Zbinden, D., Rinaldi, A. P., Urpi, L. & Wiemer, S. On the physics-based processes behind production-induced seismicity in natural gas fields. *J. Geophys. Res. Solid Earth* **122**, 3792–3812 (2017).
52. Frohlich, C. & Brunt, M. Two-year survey of earthquakes and injection/production wells in the Eagle Ford Shale, Texas, prior to the MW4.8 20 October 2011 earthquake. *Earth Planet. Sci. Lett.* **379**, 56–63 (2013).
53. De Waal, J., Muntendam-Bos, A. & Roest, J. Production induced subsidence and seismicity in the Groningen gas field — can it be managed? *Proc. Int. Assoc. Hydrol. Sci.* **372**, 129–139 (2015).
54. van Thienen-Visser, K. & Breunese, J. Induced seismicity of the Groningen gas field: history and recent developments. *Lead. Edge* **34**, 664–671 (2015).
55. Dost, B., Ruigrok, E. & Spetzler, J. Development of seismicity and probabilistic hazard assessment for the Groningen gas field. *Neth. J. Geosci.* **96**, s235–s245 (2017).
56. Candela, T. et al. Depletion-induced seismicity at the Groningen gas field: Coulomb rate-and-state models including differential compaction effect. *J. Geophys. Res. Solid Earth* **124**, 7081–7104 (2019).
57. Bourne, S., Oates, S. & Van Elk, J. The exponential rise of induced seismicity with increasing stress levels in the Groningen gas field and its implications for controlling seismic risk. *Geophys. J. Int.* **213**, 1693–1700 (2018).
58. Aochi, H. & Burnol, A. Mechanism of the ML4.0 25 April 2016 earthquake in southwest of France in the vicinity of the Lacq gas field. *J. Seismol.* **22**, 1139–1155 (2018).
59. Bardainne, T., Dubos-Sallée, N., Sénéchal, G., Gaillet, P. & Perroud, H. Analysis of the induced seismicity of the Lacq gas field (southwestern France) and model of deformation. *Geophys. J. Int.* **172**, 1151–1162 (2008).
60. Healy, J., Rubey, W., Griggs, D. & Raleigh, C. The Denver earthquakes. *Science* **161**, 1301–1310 (1968).
61. Langenbruch, C., Weingarten, M. & Zoback, M. D. Physics-based forecasting of man-made earthquake hazards in Oklahoma and Kansas. *Nat. Commun.* **9**, 3946 (2018).
62. Keranen, K. M., Weingarten, M., Abers, G. A., Bekins, B. A. & Ge, S. Sharp increase in central Oklahoma seismicity since 2008 induced by massive wastewater injection. *Science* **345**, 448–451 (2014).
63. Langenbruch, C. & Zoback, M. D. How will induced seismicity in Oklahoma respond to decreased saltwater injection rates? *Sci. Adv.* **2**, e1601542 (2016).
64. Hennings, P. H. et al. Pore pressure threshold and fault slip potential for induced earthquakes in the Dallas–Fort Worth area of North Central Texas. *Geophys. Res. Lett.* **48**, e2021GL093564 (2021).
65. Block, L. V., Wood, C. K., Yeck, W. L. & King, V. M. Induced seismicity constraints on subsurface geological structure, Paradox Valley, Colorado. *Geophys. J. Int.* **200**, 1172–1195 (2015).
66. Yeo, I. W., Brown, M. R. M., Ge, S. & Lee, K. K. Causal mechanism of injection-induced earthquakes through the Mw 5.5 Pohang earthquake case study. *Nat. Commun.* **11**, 2614 (2020).
67. Igonin, N., Verdon, J. P., Kendall, J.-M. & Eaton, D. W. Large-scale fracture systems are permeable pathways for fault activation during hydraulic fracturing. *J. Geophys. Res. Solid Earth* **126**, e2020JB020311 (2021).
68. Lei, X., Wang, Z. & Su, J. The December 2018 ML 5.7 and January 2019 ML 5.3 earthquakes in South Sichuan basin induced by shale gas hydraulic fracturing. *Seismol. Res. Lett.* **90**, 1099–1110 (2019).
69. Schultz, R., Wang, R., Gu, Y. J., Haug, K. & Atkinson, G. A seismological overview of the induced earthquakes in the Duvernay play near Fox Creek, Alberta. *J. Geophys. Res. Solid Earth* **122**, 492–505 (2017).
70. Skoumal, R. J., Brudzinski, M. R. & Currie, B. S. Proximity of Precambrian basement affects the likelihood of induced seismicity in the Appalachian, Illinois, and Williston Basins, central and eastern United States. *Geosphere* **14**, 1365–1379 (2018).
71. Zhai, G., Shirzaei, M. & Manga, M. Widespread deep seismicity in the Delaware basin, Texas, is mainly driven by shallow wastewater injection. *Proc. Natl Acad. Sci. USA* **118**, e2102338118 (2021).
72. Yang, H. et al. A shallow shock: the 25 February 2019 ML 4.9 earthquake in the Weiyuan shale gas field in Sichuan, China. *Seismol. Res. Lett.* **91**, 3182–3194 (2020).
73. Segall, P. & Lu, S. Injection-induced seismicity: poroelastic and earthquake nucleation effects. *J. Geophys. Res. Solid Earth* **120**, 5082–5103 (2015).
74. Deng, K., Liu, Y. & Harrington, R. M. Poroelastic stress triggering of the December 2013 Crooked Lake, Alberta, induced seismicity sequence. *Geophys. Res. Lett.* **43**, 8482–8491 (2016).
75. Kettlety, T. & Verdon, J. P. Fault triggering mechanisms for hydraulic fracturing-induced seismicity from the Preston New Road, UK case study. *Front. Earth Sci.* **9**, 382 (2021).
76. Meng, Q., Ni, S. & Peng, Z. Complex source behaviors and spatio-temporal evolution of seismicity during the 2015–2016 earthquake sequence in Cushing, Oklahoma. *J. Geophys. Res. Solid Earth* **126**, e2021JB022168 (2021).
77. Vidale, J. E., Agnew, D. C., Johnston, M. J. & Oppenheimer, D. H. Absence of earthquake correlation with Earth tides: an indication of high preseismic fault stress rate. *J. Geophys. Res. Solid Earth* **103**, 24567–24572 (1998).
78. Chang, K. W., Yoon, H., Kim, Y. & Lee, M. Y. Operational and geological controls of coupled poroelastic stressing and pore-pressure accumulation along faults: induced earthquakes in Pohang, South Korea. *Sci. Rep.* **10**, 2073 (2020).
79. Zbinden, D., Rinaldi, A. P., Diehl, T. & Wiemer, S. Hydromechanical modeling of fault reactivation in the St. Gallen Deep Geothermal Project (Switzerland): poroelasticity or hydraulic connection? *Geophys. Res. Lett.* **47**, e2019GL085201 (2020).
80. Zhai, G., Shirzaei, M., Manga, M. & Chen, X. Pore-pressure diffusion, enhanced by poroelastic stresses, controls induced seismicity in Oklahoma. *Proc. Natl Acad. Sci. USA* **116**, 16228–16233 (2019).
81. Goebel, T., Weingarten, M., Chen, X., Haffener, J. & Brodsky, E. The 2016 Mw5.1 Fairview, Oklahoma earthquakes: evidence for long-range poroelastic triggering at >40 km from fluid disposal wells. *Earth Planet. Sci. Lett.* **472**, 50–61 (2017).
82. Jiang, G., Liu, L., Barbour, A. J., Lu, R. & Yang, H. Physics-based evaluation of the maximum magnitude of potential earthquakes induced by the Hutubi (China) underground gas storage. *J. Geophys. Res. Solid Earth* **126**, e2020JB021379 (2021).
83. Pennington, W. D., Davis, S. D., Carlson, S. M., DuPree, J. & Ewing, T. E. The evolution of seismic barriers and asperities caused by the depressuring of fault planes in oil and gas fields of south Texas. *Bull. Seismol. Soc. Am.* **76**, 939–948 (1986).
84. Segall, P. & Fitzgerald, S. D. A note on induced stress changes in hydrocarbon and geothermal reservoirs. *Tectonophysics* **289**, 117–128 (1998).
85. Candela, T., Wassing, B., Ter Heege, J. & Buijze, L. How earthquakes are induced. *Science* **360**, 598–600 (2018).
86. Dempsey, D. & Suckale, J. Physics-based forecasting of induced seismicity at Groningen gas field, the Netherlands. *Geophys. Res. Lett.* **44**, 7773–7782 (2017).
87. Deng, F., Dixon, T. H. & Xie, S. Surface deformation and induced seismicity due to fluid injection and oil and gas extraction in western Texas. *J. Geophys. Res. Solid Earth* **125**, e2019JB018962 (2020).
88. Segall, P., Grasso, J.-R. & Mossop, A. Poroelastic stressing and induced seismicity near the Lacq gas field, southwestern France. *J. Geophys. Res. Solid Earth* **99**, 15423–15438 (1994).
89. Dahm, T. et al. The 2004 Mw 4.4 Rotenburg, Northern Germany, earthquake and its possible relationship with gas recovery. *Bull. Seismol. Soc. Am.* **97**, 691–704 (2007).
90. Villarrasa Ríaño, V., Carrera, J., Olivella, S., Rutqvist, J. & Laloui, L. Induced seismicity in geologic carbon storage. *Solid Earth* **10**, 871–892 (2019).
91. De Simone, S., Carrera, J. & Villarrasa, V. Superposition approach to understand triggering mechanisms of post-injection induced seismicity. *Geothermics* **70**, 85–97 (2017).
92. Izadi, G. & Elsworth, D. The effects of thermal stress and fluid pressure on induced seismicity during stimulation to production within fractured reservoirs. *Terra Nova* **25**, 374–380 (2013).
93. Kivi, I. R., Pujades, E., Rutqvist, J. & Villarrasa, V. Cooling-induced reactivation of distant faults during long-term geothermal energy production in hot sedimentary aquifers. *Sci. Rep.* **12**, 2065 (2022).

94. Kwiatek, G. et al. Effects of long-term fluid injection on induced seismicity parameters and maximum magnitude in northwestern part of the Geysers geothermal field. *J. Geophys. Res. Solid Earth* **120**, 7085–7101 (2015).
95. Bruehl, D. Impact of induced thermal stresses during circulation tests in an engineered fractured geothermal reservoir: example of the Soultz-sous-Forêts European hot fractured rock geothermal project, Rhine Graben, France. *Oil Gas Sci. Technol.* **57**, 459–470 (2002).
96. Martínez-Garzón, P. et al. Spatiotemporal changes, faulting regimes, and source parameters of induced seismicity: a case study from the Geysers geothermal field. *J. Geophys. Res. Solid Earth* **119**, 8378–8396 (2014).
97. Jeanne, P., Rutqvist, J. & Dobson, P. F. Influence of injection-induced cooling on deviatoric stress and shear reactivation of preexisting fractures in enhanced geothermal systems. *Geothermics* **70**, 367–375 (2017).
98. Vilarrasa, V., Rinaldi, A. P. & Rutqvist, J. Long-term thermal effects on injectivity evolution during CO₂ storage. *Int. J. Greenh. Gas Control* **64**, 314–322 (2017).
99. Stein, R. S. The role of stress transfer in earthquake occurrence. *Nature* **402**, 605–609 (1999).
100. Hardebeck, J. L. & Harris, R. A. Earthquakes in the shadows: why aftershocks occur at surprising locations. *Seismic Rec.* **2**, 207–216 (2022).
101. Dieterich, J. H. Earthquake nucleation on faults with rate-and state-dependent strength. *Tectonophysics* **211**, 115–134 (1992).
102. Dieterich, J. H., Richards-Dinger, K. B. & Kroll, K. A. Modeling injection-induced seismicity with the physics-based earthquake simulator RSQSim. *Seismol. Res. Lett.* **86**, 1102–1109 (2015).
103. Kettlety, T., Verdon, J. P., Werner, M. J., Kendall, J. M. & Budge, J. Investigating the role of elastostatic stress transfer during hydraulic fracturing-induced fault activation. *Geophys. J. Int.* **217**, 1200–1216 (2019).
104. Catalli, F., Meier, M.-A. & Wiemer, S. The role of Coulomb stress changes for injection-induced seismicity: the Basel enhanced geothermal system. *Geophys. Res. Lett.* **40**, 72–77 (2013).
105. Schoenball, M., Baujard, C., Kohl, T. & Dorbath, L. The role of triggering by static stress transfer during geothermal reservoir stimulation. *J. Geophys. Res. Solid Earth*, **117**, B09307 (2012).
106. Catalli, F., Rinaldi, A. P., Gischig, V., Nespoli, M. & Wiemer, S. The importance of earthquake interactions for injection-induced seismicity: retrospective modeling of the Basel enhanced geothermal system. *Geophys. Res. Lett.* **43**, 4992–4999 (2016).
107. Peña Castro, A. F. et al. Stress chatter via fluid flow and fault slip in a hydraulic fracturing-induced earthquake sequence in the Montney Formation, British Columbia. *Geophys. Res. Lett.* **47**, e2020GL087254 (2020).
108. Wang, J. et al. Sequential fault reactivation and secondary triggering in the March 2019 Red Deer induced earthquake swarm. *Geophys. Res. Lett.* **47**, e2020GL090219 (2020).
109. Verdecchia, A., Cochran, E. S. & Harrington, R. M. Fluid-earthquake and earthquake-earthquake interactions in Southern Kansas, USA. *J. Geophys. Res. Solid Earth* **126**, e2020JB020384 (2021).
110. Chen, X. et al. The Pawnee earthquake as a result of the interplay among injection, faults and foreshocks. *Sci. Rep.* **7**, 1–18 (2017).
111. Cao, W., Shi, J.-Q., Durucan, S. & Korre, A. Evaluation of shear slip stress transfer mechanism for induced microseismicity at In Salah CO₂ storage site. *Int. J. Greenh. Gas Control* **107**, 103302 (2021).
112. Scholz, C. H. *The Mechanics of Earthquakes and Faulting* (Cambridge Univ. Press, 2002).
113. Johnston, M., Borchardt, R., Linde, A. & Gladwin, M. Continuous borehole strain and pore pressure in the near field of the 28 September 2004 M 6.0 Parkfield, California, earthquake: implications for nucleation, fault response, earthquake prediction, and tremor. *Bull. Seismol. Soc. Am.* **96**, S56–S72 (2006).
114. Eyre, T. S. et al. The role of aseismic slip in hydraulic fracturing-induced seismicity. *Sci. Adv.* **5**, eaav7172 (2019).
115. Cornet, F. H. Seismic and aseismic motions generated by fluid injections. *Geomech. Energy Environ.* **5**, 42–54 (2016).
116. Guglielmi, Y., Cappa, F., Avouac, J.-P., Henry, P. & Elsworth, D. Seismicity triggered by fluid injection-induced aseismic slip. *Science* **348**, 1224–1226 (2015).
117. Bhattacharya, P. & Viesca, R. C. Fluid-induced aseismic fault slip outpaces pore-fluid migration. *Science* **364**, 464–468 (2019).
118. Wei, S. et al. The 2012 Brawley swarm triggered by injection-induced aseismic slip. *Earth Planet. Sci. Lett.* **422**, 115–125 (2015).
119. Bourouis, S. & Bernard, P. Evidence for coupled seismic and aseismic fault slip during water injection in the geothermal site of Soultz (France), and implications for seismic transients. *Geophys. J. Int.* **169**, 723–732 (2007).
120. Sone, H. & Zoback, M. D. Time-dependent deformation of shale gas reservoir rocks and its long-term effect on the in situ state of stress. *Int. J. Rock Mech. Min. Sci.* **69**, 120–132 (2014).
121. Hettner, M. H. H., Schutjens, P. M. T. M., Verboom, B. J. M. & Gussinklo, H. J. Production-induced compaction of a sandstone reservoir: the strong influence of stress path. *SPE Reserv. Eval. Eng.* **3**, 342–347 (2000).
122. Hettner, M., Papamichos, E. & Schutjens, P. Subsidence delay: field observations and analysis. *Oil Gas Sci. Technol.* **57**, 443–458 (2002).
123. van Wees, J.-D., Osinga, S., Van Thienen-Visser, K. & Fokker, P. A. Reservoir creep and induced seismicity: inferences from geomechanical modeling of gas depletion in the Groningen field. *Geophys. J. Int.* **212**, 1487–1497 (2017).
124. Meller, C. & Kohl, T. The significance of hydrothermal alteration zones for the mechanical behavior of a geothermal reservoir. *Geotherm. Energy* **2**, 12 (2014).
125. Rohmer, J., Pluymakers, A. & Renard, F. Mechano-chemical interactions in sedimentary rocks in the context of CO₂ storage: weak acid, weak effects? *Earth Sci. Rev.* **157**, 86–110 (2016).
126. Westaway, R. & Burnside, N. M. Fault 'corrosion' by fluid injection: a potential cause of the November 2017 5.5 Korean Earthquake. *Geofluids* **2019**, 1280721 (2019).
127. Di Toro, G. et al. Fault lubrication during earthquakes. *Nature* **471**, 494–498 (2011).
128. Zoback, M. D. *Reservoir Geomechanics* (Cambridge Univ. Press, 2010).
129. van den Ende, M. P. A. & Niemeijer, A. R. An investigation into the role of time-dependent cohesion in interseismic fault restrengthening. *Sci. Rep.* **9**, 9894 (2019).
130. Shapiro, S. A. & Dinske, C. Stress drop, seismogenic index and fault cohesion of fluid-induced earthquakes. *Rock Mech. Rock Eng.* **54**, 5483–5492 (2021).
131. Bachmann, C. E., Wiemer, S., Goertz-Allmann, B. & Woessner, J. Influence of pore-pressure on the event-size distribution of induced earthquakes. *Geophys. Res. Lett.* **39**, 9302 (2012).
132. Stokes, S. M. et al. Pore pressure diffusion and onset of induced seismicity. *J. Geophys. Res. Solid Earth* **128**, e2022JB026012 (2023).
133. Ge, S. & Saar, M. O. Review: induced seismicity during geoelectricity development — a hydromechanical perspective. *J. Geophys. Res. Solid Earth* **127**, e2021JB023141 (2022).
134. Shapiro, S. A., Dinske, C., Langenbruch, C. & Wenzel, F. Seismogenic index and magnitude probability of earthquakes induced during reservoir fluid stimulations. *Lead. Edge* **29**, 304–309 (2010).
135. Kao, H. et al. Induced seismicity in western Canada linked to tectonic strain rate: implications for regional seismic hazard. *Geophys. Res. Lett.* **45**, 11,104–11,115 (2018).
136. Langenbruch, C., Ellsworth, W. L., Woo, J.-U. & Wald, D. J. Value at induced risk: injection-induced seismic risk from low-probability, high-impact events. *Geophys. Res. Lett.* **47**, e2019GL085878 (2020).
137. Lee, K.-K. et al. Managing injection-induced seismic risks. *Science* **364**, 730–732 (2019).
138. van der Elst, N. J., Page, M. T., Weiser, D. A., Goebel, T. H. W. & Hosseini, S. M. Induced earthquake magnitudes are as large as (statistically) expected. *J. Geophys. Res. Solid Earth* **121**, 4575–4590 (2016).
139. Mousavi, S. M., Ogwari, P. O., Horton, S. P. & Langston, C. A. Spatio-temporal evolution of frequency-magnitude distribution and seismogenic index during initiation of induced seismicity at Guy-Graben, Arkansas. *Phys. Earth Planet. Inter.* **267**, 53–66 (2017).
140. Eaton, D. W. & Maghsoudi, S. 2b... or not 2b? Interpreting magnitude distributions from microseismic catalogs. *First Break*, **33**, 10 (2015).
141. Shapiro, S. A. Seismogenic index of underground fluid injections and productions. *J. Geophys. Res. Solid Earth* **123**, 7983–7997 (2018).
142. Shapiro, S. A. *Fluid-Induced Seismicity* (Cambridge Univ. Press, 2015).
143. Grigoratos, I., Rathje, E., Bazzurro, P. & Savvaidis, A. Earthquakes induced by wastewater injection, part II: statistical evaluation of causal factors and seismicity rate forecasting. *Bull. Seismol. Soc. Am.* **110**, 2483–2497 (2020).
144. Cacace, M., Hofmann, H. & Shapiro, S. A. Projecting seismicity induced by complex alterations of underground stresses with applications to geothermal systems. *Sci. Rep.* **11**, 23560 (2021).
145. Sumy, D. F., Cochran, E. S., Keranen, K. M., Wei, M. & Abers, G. A. Observations of static Coulomb stress triggering of the November 2011 M5.7 Oklahoma earthquake sequence. *J. Geophys. Res. Solid Earth* **119**, 1904–1923 (2014).
146. Shapiro, S. A., Krüger, O. S. & Dinske, C. Probability of inducing given-magnitude earthquakes by perturbing finite volumes of rocks. *J. Geophys. Res. Solid Earth* **118**, 3557–3575 (2013).
147. Afshari Moein, M. J., Tormann, T., Valley, B. & Wiemer, S. Maximum magnitude forecast in hydraulic stimulation based on clustering and size distribution of early microseismicity. *Geophys. Res. Lett.* **45**, 6907–6917 (2018).
148. McGarr, A. Maximum magnitude earthquakes induced by fluid injection. *J. Geophys. Res. Solid Earth* **119**, 1008–1019 (2014).
149. Ellsworth, W. L., Giardini, D., Townsend, J., Ge, S. & Shimamoto, T. Triggering of the Pohang, Korea, earthquake (Mw 5.5) by enhanced geothermal system stimulation. *Seismol. Res. Lett.* **90**, 1844–1858 (2019).
150. Galis, M., Ampuero, J. P., Mai, P. M. & Cappa, F. Induced seismicity provides insight into why earthquake ruptures stop. *Sci. Adv.* **3**, eaap7528 (2017).
151. Ciardo, F. & Rinaldi, A. P. Impact of injection rate ramp-up on nucleation and arrest of dynamic fault slip. *Geomech. Geophys. Geo-Energy Geo-Resour.* **8**, 28 (2021).
152. Langenbruch, C., Moein, M. J. A. & Shapiro, S. A. In *Fall Meeting 2022* (AGU).
153. Grigoratos, I., Rathje, E., Bazzurro, P. & Savvaidis, A. Earthquakes induced by wastewater injection, part I: model development and hindcasting. *Bull. Seismol. Soc. Am.* **110**, 2466–2482 (2020).
154. Langenbruch, C., Moein, M. J. & Shapiro, S. A. *Pressure Diffusion Controls Maximum Induced Earthquake Magnitudes* (Copernicus Meetings, 2023).
155. Gischig, V. S. Rupture propagation behavior and the largest possible earthquake induced by fluid injection into deep reservoirs. *Geophys. Res. Lett.* **42**, 7420–7428 (2015).
156. Lee, E. J., Liao, W. Y., Mu, D., Wang, W. & Chen, P. GPU-accelerated automatic microseismic monitoring algorithm (GAMMA) and its application to the 2019 Ridgecrest earthquake sequence. *Seismol. Res. Lett.* **91**, 2062–2074 (2020).
157. Wang, R. et al. Injection-induced earthquakes on complex fault zones of the Raton Basin illuminated by machine-learning phase picker and dense nodal array. *Geophys. Res. Lett.* **47**, e2020GL088168 (2020).

158. Broccardo, M., Mignan, A., Wiemer, S., Stojadinovic, B. & Giardini, D. Hierarchical Bayesian modeling of fluid-induced seismicity. *Geophys. Res. Lett.* **44**, 11,357–11,367 (2017).
159. Foulger, G. et al. Human-induced earthquakes: E-PIE — a generic tool for evaluating proposals of induced earthquakes. *J. Seismol.* **27**, 21–44 (2023).
160. Davis, S. D. & Frohlich, C. Did (or will) fluid injection cause earthquakes? Criteria for a rational assessment. *Seismol. Res. Lett.* **64**, 207–224 (1993).
161. Wang, B., Kao, H., Yu, H., Visser, R. & Verdecchia, A. Quantitative evaluation of the competing effects of wastewater disposal and hydraulic fracturing on causing induced earthquakes: a case study of an M3.1 earthquake sequence in Western Canada. *J. Geophys. Res. Solid Earth* **128**, e2022JB025048 (2023).
162. Bommer, J. J. Earthquake hazard and risk analysis for natural and induced seismicity: towards objective assessments in the face of uncertainty. *Bull. Earthq. Eng.* **20**, 2825–3069 (2022).
163. Ghofrani, H., Atkinson, G. M., Schultz, R. & Assatourians, K. Short-term hindcasts of seismic hazard in the Western Canada sedimentary basin caused by induced and natural earthquakes. *Seismol. Res. Lett.* **90**, 1420–1435 (2019).
164. Bentz, S., Kwiatek, G., Martínez-Garzón, P., Bohnhoff, M. & Dresen, G. Seismic moment evolution during hydraulic stimulations. *Geophys. Res. Lett.* **47**, e2019GL086185 (2020).
165. Langenbruch, C. & Shapiro, S. A. Decay rate of fluid-induced seismicity after termination of reservoir stimulations. *Geophysics* **75**, MA53–MA62 (2010).
166. Kim, T. & Avouac, J. P. Stress-based and convolutional forecasting of injection-induced seismicity: application to the Otaniemi geothermal reservoir stimulation. *J. Geophys. Res. Solid Earth* **128**, e2022JB024960 (2023).
167. Dieterich, J. A constitutive law for rate of earthquake production and its application to earthquake clustering. *J. Geophys. Res. Solid Earth* **99**, 2601–2618 (1994).
168. Hager, B. H. et al. A process-based approach to understanding and managing triggered seismicity. *Nature* **595**, 684–689 (2021).
169. Bourne, S. J. & Oates, S. J. Development of statistical geomechanical models for forecasting seismicity induced by gas production from the Groningen field. *Neth. J. Geosci.* **96**, s175–s182 (2017).
170. Rinaldi, A. P. & Nespoli, M. TOUGH2-seed: a coupled fluid flow and mechanical-stochastic approach to model injection-induced seismicity. *Comput. Geosci.* **108**, 86–97 (2017).
171. Beroza, G. C., Segou, M. & Mostafa Mousavi, S. Machine learning and earthquake forecasting — next steps. *Nat. Commun.* **12**, 4761 (2021).
172. Qin, Y., Chen, T., Ma, X. & Chen, X. Forecasting induced seismicity in Oklahoma using machine learning methods. *Sci. Rep.* **12**, 9319 (2022).
173. Yu, P. et al. Association between injection and microseismicity in geothermal fields with multiple wells: data-driven modelling of Rotokawa, New Zealand, and Húsulí, Iceland. *J. Geophys. Res. Solid Earth* **128**, e2022JB025952 (2023).
174. Rouet-Leduc, B. et al. Machine learning predicts laboratory earthquakes. *Geophys. Res. Lett.* **44**, 9276–9282 (2017).
175. Feng, Y., Mignan, A., Sornette, D. & Gao, K. Investigating injection pressure as a predictor to enhance real-time forecasting of fluid-induced seismicity: a Bayesian model comparison. *Seismol. Soc. Am.* **94**, 708–719 (2023).
176. Schultz, R., Ellsworth, W. L. & Beroza, G. C. An ensemble approach to characterizing trailing-induced seismicity. *Seismol. Res. Lett.* **94**, 699–707 (2023).
177. Marzocchi, W., Zecher, J. D. & Jordan, T. H. Bayesian forecast evaluation and ensemble earthquake forecasting. *Bull. Seismol. Soc. Am.* **102**, 2574–2584 (2012).
178. Bommer, J. J. et al. Control of hazard due to seismicity induced by a hot fractured rock geothermal project. *Eng. Geol.* **83**, 287–306 (2006).
179. Schultz, R., Beroza, G. C. & Ellsworth, W. L. A strategy for choosing red-light thresholds to manage hydraulic fracturing induced seismicity in North America. *J. Geophys. Res. Solid Earth* **126**, e2021JB022340 (2021).
180. Ader, T. et al. Design and implementation of a traffic light system for deep geothermal well stimulation in Finland. *J. Seismol.* **24**, 991–1014 (2020).
181. Verdon, J. P. & Bommer, J. J. Green, yellow, red, or out of the blue? An assessment of traffic light schemes to mitigate the impact of hydraulic fracturing-induced seismicity. *J. Seismol.* **25**, 301–326 (2021).
182. Schultz, R., Ellsworth, W. L. & Beroza, G. C. Statistical bounds on how induced seismicity stops. *Sci. Rep.* **12**, 1184 (2022).
183. Alghannam, M. & Juanes, R. Understanding rate effects in injection-induced earthquakes. *Nat. Commun.* **11**, 3053 (2020).
184. Qiu, Y., Adams, M. & Grasselli, G. In *SPE Annual Technical Conference and Exhibition* (OnePetro, 2023).
185. Weingarten, M., Ge, S., Godt, J. W., Bekins, B. A. & Rubinstein, J. L. High-rate injection is associated with the increase in US mid-continent seismicity. *Science* **348**, 1336–1340 (2015).
186. Wang, L. et al. Laboratory study on fluid-induced fault slip behavior: the role of fluid pressurization rate. *Geophys. Res. Lett.* **47**, e2019GL086627 (2020).
187. Muntendam-Bos, A. G. et al. An overview of induced seismicity in the Netherlands. *Neth. J. Geosci.* **101**, e1 (2022).
188. Frash, L. P. et al. Fracture caging to limit induced seismicity. *Geophys. Res. Lett.* **48**, e2020GL090648 (2021).
189. Zang, A., Yoon, J. S., Stephansson, O. & Heidbach, O. Fatigue hydraulic fracturing by cyclic reservoir treatment enhances permeability and reduces induced seismicity. *Geophys. J. Int.* **195**, 1282–1287 (2013).
190. Stefanou, I. Controlling anthropogenic and natural seismicity: insights from active stabilization of the spring-slider model. *J. Geophys. Res. Solid Earth* **124**, 8786–8802 (2019).
191. Gutiérrez-Oribio, D., Tzortzopoulos, G., Stefanou, I. & Plestan, F. Earthquake control: an emerging application for robust control. Theory and experimental tests. *IEEE Trans. Control Syst. Technol.* **31**, 1747–1761 (2023).
192. Leptokaropoulos, K. et al. IS-EPOS: a platform for anthropogenic seismicity research. *Acta Geophys.* **67**, 299–310 (2019).
193. Liu, G. et al. Detailed imaging of a seismogenic fault that potentially induced the two 2019 Wei yuan moderate earthquakes in the Sichuan basin, China. *Seismol. Soc. Am.* **94**, 1379–1391 (2023).
194. Jin, G. & Roy, B. Hydraulic-fracture geometry characterization using low-frequency DAS signal. *Lead. Edge* **36**, 975–980 (2017).
195. Pepin, K. S., Ellsworth, W. L., Sheng, Y. & Zebker, H. A. Shallow aseismic slip in the Delaware basin determined by Sentinel-1 InSAR. *J. Geophys. Res. Solid Earth* **127**, e2021JB023157 (2022).
196. Wang, T. A. & Dunham, E. M. Hindcasting injection-induced aseismic slip and microseismicity at the cooper basin enhanced geothermal systems project. *Sci. Rep.* **12**, 19481 (2022).
197. Yu, H., Kao, H., Wang, B. & Visser, R. Long-term fluid injection can expedite fault reactivation and development: Riedel shear structures illuminated by induced earthquakes in Alberta, Canada. *J. Geophys. Res. Solid Earth* **127**, e2022JB025126 (2022).
198. Li, T. et al. Earthquakes induced by wastewater disposal near Musreau Lake, Alberta, 2018–2020. *Seismol. Res. Lett.* **93**, 727–738 (2021).
199. Yu, H., Kao, H., Visser, R. & Wang, B. From seismic quiescence to surged activity after decades of wastewater disposal: a case study in Central-West Alberta, Canada. *Geophys. Res. Lett.* **48**, e2021GL095074 (2021).
200. Hennings, P. H. & Young, M. H. *Recent Seismicity in the Southern Midcontinent, USA: Scientific, Regulatory, and Industry Responses* (Geological Society of America, 2023).
201. Walsh, F. R. III & Zoback, M. D. Probabilistic assessment of potential fault slip related to injection-induced earthquakes: application to north-central Oklahoma, USA. *Geology* **44**, 991–994 (2016).
202. Savvaidis, A., Lomax, A. & Breton, C. Induced seismicity in the Delaware basin, West Texas, is caused by hydraulic fracturing and wastewater disposal. *Bull. Seismol. Soc. Am.* **110**, 2225–2241 (2020).
203. Cesca, S. et al. Reply to: multiple induced seismicity mechanisms at Castor underground gas storage illustrate the need for thorough monitoring. *Nat. Commun.* **13**, 3445 (2022).
204. Vilarrasa, V., De Simone, S., Carrera, J. & Villaseñor, A. Multiple induced seismicity mechanisms at Castor underground gas storage illustrate the need for thorough monitoring. *Nat. Commun.* **13**, 3447 (2022).
205. Lellouch, A., Schultz, R., Lindsey, N. J., Biondi, B. L. & Ellsworth, W. L. Low-magnitude seismicity with a downhole distributed acoustic sensing array — examples from the FORGE geothermal experiment. *J. Geophys. Res. Solid Earth* **126**, e2020JB020462 (2021).
206. Lecoulant, J., Ma, Y., Dettmer, J. & Eaton, D. Strain-based forward modeling and inversion of seismic moment tensors using distributed acoustic sensing (DAS) observations. *Front. Earth Sci.* **11**, 1176921 (2023).
207. Ji, Y., Hofmann, H., Duan, K. & Zang, A. Laboratory experiments on fault behavior towards better understanding of injection-induced seismicity in geoelectric systems. *Earth Sci. Rev.* **226**, 103916 (2022).
208. Hofmann, H., Zimmermann, G., Zang, A. & Min, K.-B. Cyclic soft stimulation (CSS): a new fluid injection protocol and traffic light system to mitigate seismic risks of hydraulic stimulation treatments. *Geotherm. Energy* **6**, 27 (2018).
209. Meng, M. et al. Hydro-mechanical measurements of sheared crystalline rock fractures with applications for EGS collab experiments 1 and 2. *J. Geophys. Res. Solid Earth* **127**, e2021JB023000 (2022).
210. Degen, D., Cacace, M. & Wellmann, F. 3D multi-physics uncertainty quantification using physics-based machine learning. *Sci. Rep.* **12**, 17491 (2022).
211. Afshari Moen, M. J. et al. Fracture network characterization using stress-based tomography. *J. Geophys. Res. Solid Earth* **123**, 9324–9340 (2018).
212. Ahlers, S. et al. 3D crustal stress state of Germany according to a data-calibrated geomechanical model. *Solid Earth* **12**, 1777–1799 (2021).
213. Baisch, S. et al. Continued geothermal reservoir stimulation experiments in the cooper basin (Australia). *Bull. Seismol. Soc. Am.* **105**, 198–209 (2015).
214. Li, W., Ni, S., Zang, C. & Chu, R. Rupture directivity of the 2019 Mw 5.8 Changning, Sichuan, China, earthquake and implication for induced seismicity. *Bull. Seismol. Soc. Am.* **110**, 2138–2153 (2020).
215. Babaia Mahani, A. et al. Ground-motion characteristics of the 30 November 2018 injection-induced earthquake sequence in northeast British Columbia, Canada. *Seismol. Res. Lett.* **90**, 1457–1467 (2019).
216. Wilson, M. P., Foulger, G. R., Gluyas, J. G., Davies, R. J. & Julian, B. R. HiQuake: the human-induced earthquake database. *Seismol. Res. Lett.* **88**, 1560–1565 (2017).
217. Jaeger, J. C., Cook, N. G. & Zimmerman, R. *Fundamentals of Rock Mechanics*. (John Wiley & Sons, 2009).
218. McLaskey, G. C. Earthquake initiation from laboratory observations and implications for foreshocks. *J. Geophys. Res. Solid Earth* **124**, 12882–12904 (2019).

219. Dempsey, D. & Suckale, J. Collective properties of injection-induced earthquake sequences: 1. Model. description directivity bias. *J. Geophys. Res. Solid Earth* **121**, 3609–3637 (2016).
220. Doglioni, C. A classification of induced seismicity. *Geosci. Front.* **9**, 1903–1909 (2018).
221. Luu, K., Schoenball, M., Oldenburg, C. M. & Rutqvist, J. Coupled hydromechanical modeling of induced seismicity from CO₂ injection in the Illinois Basin. *J. Geophys. Res. Solid Earth* **127**, e2021JB023496 (2022).
222. Norbeck, J. & Rubinstein, J. L. Hydromechanical earthquake nucleation model forecasts onset, peak, and falling rates of induced seismicity in Oklahoma and Kansas. *Geophys. Res. Lett.* **45**, 2963–2975 (2018).
223. Walsh, F. R. & Zoback, M. D. Oklahoma's recent earthquakes and saltwater disposal. *Sci. Adv.* **1**, e1500195 (2015).

Acknowledgements

The research leading to this Review has received funding from the German Research Foundation DFG (project AF 115/1-1) and the Stanford Center for Induced and Triggered Seismicity. The authors thank the sponsors of the PHASE consortium supporting the research presented in this paper at Free University of Berlin. F.G. is supported by the UniPi PRA Project 'Fluid migration in the upper crust: from natural hazards to geo-resources' (PRA_2022_66) and by the Italian Ministry of University and Research PRIN Project 'PREVENT' (2022MJ82MC). The authors thank Seismix SRL for the permission to redraw and modify Fig. 1.

Author contributions

M.J.A.M. conceived the idea, designed and coordinated the work. M.J.A.M., C.L., R.S. and F.G. prepared the visualizations. All authors contributed to the writing of the paper. All authors reviewed and edited the manuscript before submission.

Competing interests

The authors declare no competing interests.

Additional information

Peer review information *Nature Reviews Earth & Environment* thanks P. Hennings, H. Kao and the other, anonymous, reviewer(s) for their contribution to the peer review of this work.

Publisher's note Springer Nature remains neutral with regard to jurisdictional claims in published maps and institutional affiliations.

Springer Nature or its licensor (e.g. a society or other partner) holds exclusive rights to this article under a publishing agreement with the author(s) or other rightsholder(s); author self-archiving of the accepted manuscript version of this article is solely governed by the terms of such publishing agreement and applicable law.

© Springer Nature Limited 2023